

Effective nonlocal kernels on Reaction-diffusion networks [☆]

Shin-Ichiro Ei^{a,*}, Hiroshi Ishii^a, Shigeru Kondo^b, Takashi Miura^c, Yoshitaro Tanaka^d

^a Department of Mathematics, Faculty of Science, Hokkaido University

^b Graduate School of Frontier Biosciences, Osaka University

^c Graduate School of Medical Sciences, Kyushu University

^d School of Systems Information Science, Future University Hakodate

Abstract

A new method to derive an essential integral kernel from any given reaction-diffusion network is proposed. Any network describing metabolites or signals with arbitrary many factors can be reduced to a single or a simpler system of integro-differential equations called “effective equation” including the reduced integral kernel (called “effective kernel”) in the convolution type. As one typical example, the Mexican hat shaped kernel is theoretically derived from two component activator-inhibitor systems. It is also shown that a three component system with quite different appearance from activator-inhibitor systems is reduced to an effective equation with the Mexican hat shaped kernel. It means that the two different systems have essentially the same effective equations and that they exhibit essentially the same spatial and temporal patterns. Thus, we can identify two different systems with the understanding in unified concept through the reduced effective kernels. Other two applications of this method are also given: Applications to pigment patterns on skins (two factors network with long range interaction) and waves of differentiation (called proneural waves) in visual systems on brains (four factors network with long range interaction). In the applications, we observe the reproduction of the same spatial and temporal patterns as those appearing in pre-existing models through the numerical simulations of the effective equations.

Keywords: non-local convolution, pattern formation, network, reaction-diffusion, Turing pattern

45K05, 35Q92, 92C42

1. Introduction

The understanding of the mechanism for self-organization is one of the most attractive and important themes in biology. Diffusion driven instability proposed by Turing [21] has given a

[☆]This work was supported in part by JST CREST (No. JPMJCR14D3) to S.-I. E., JSPS KAKENHI (No. 17K14228) to Y. T.

*Corresponding author. E-mail: Eichiro@math.sci.hokudai.ac.jp

Email addresses: Eichiro@math.sci.hokudai.ac.jp (Shin-Ichiro Ei),
hiroshi-ishii@eis.hokudai.ac.jp (Hiroshi Ishii), skondo@fbs.osaka-u.ac.jp (Shigeru Kondo),
miura_t@anat1.med.kyushu-u.ac.jp (Takashi Miura), yoshitaro.tanaka@gmail.com (Yoshitaro Tanaka)

Preprint submitted to Elsevier

February 2, 2022

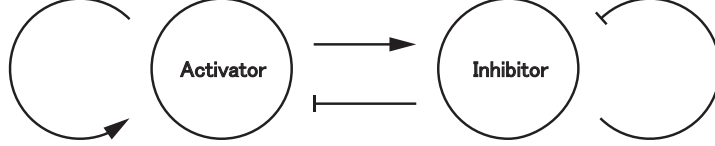


Figure 1: Activator-Inhibitor network. \rightarrow and \dashv denote activation and inhibition, respectively.

significant part of the theoretical basement which has been adapted by many works related to pattern formation problems (Meinhardt [11], Murray [13]). In practice, the existence of the mechanism in real nature has been observed and checked for several real phenomena (e.g. Ouyang and Swinney [17], Kondo and Asai [9], Yamaguchi et.al. [23]). The mechanism of the diffusion driven instability was understood as the interaction between the slow diffusivity of short range self-enhancing activator and the fast one of long range inhibitor or simply “local activation with long-range inhibition (LALI)” (e.g. Gierer-Meinhardt [7], Oster [16]) as in Fig.1. The situation is frequently modeled in the form of reaction-diffusion systems with two components of the activator $u = u(t, x)$ and the inhibitor $v = v(t, x)$ at time $t > 0$ and position x

$$\begin{cases} u_t &= d_1 \Delta u + f(u, v), \\ v_t &= d_2 \Delta v + g(u, v), \end{cases} \quad (1.1)$$

which is called Activator-Inhibitor system. In (1.1), Δ denotes the Laplace operator and it is assumed that the diffusion coefficients $0 < d_1 < d_2$ and the nonlinear terms $f_u > 0$, $f_v < 0$, $g_u > 0$ and $g_v < 0$. The typical example of f and g are $f(u, v) = c_1 u - c_2 v$ and $g(u, v) = c_3 u - c_4 v$ with all positive constants c_j , ($j = 1, \dots, 4$), which appear as a linear approximation in the neighbourhood of an equilibrium. In fact, the diffusion driven instability is understood for the linearized system as follows: Let the linearized system for an equilibrium, say 0, be

$$\begin{cases} u_t &= d_1 \Delta u + c_1 u - c_2 v, \\ v_t &= d_2 \Delta v + c_3 u - c_4 v. \end{cases} \quad (1.2)$$

For the simplicity, we consider (1.2) on \mathbf{R}^1 . Then the Fourier transformation of (1.2) yields

$$\begin{cases} \hat{u}_t &= -d_1 \xi^2 \hat{u} + c_1 \hat{u} - c_2 \hat{v}, \\ \hat{v}_t &= -d_2 \xi^2 \hat{v} + c_3 \hat{u} - c_4 \hat{v} \end{cases} \quad (1.3)$$

while the specific notations are defined in Section 2. That is, (1.3) is written as $\hat{U}_t = B(\xi) \hat{U}$ with $\hat{U} := \begin{pmatrix} \hat{u} \\ \hat{v} \end{pmatrix}$ and $B(\xi) := \begin{pmatrix} -d_1 \xi^2 + c_1 & -c_2 \\ c_3 & -d_2 \xi^2 - c_4 \end{pmatrix}$. Denoting the eigenvalues of $B(\xi)$ by $\lambda_1(\xi)$, $\lambda_2(\xi)$ with $\lambda_1(0) \geq \lambda_2(0)$ and defining $\lambda_{max}(\xi) := \max\{\lambda_1(\xi), \lambda_2(\xi)\}$, we assume the maximal eigenvalue $\lambda_{max}(\xi)$ satisfies $\lambda_{max}(0) < 0$ and $\lambda_{max}(\xi_1) > 0$ for $\xi_1 > 0$ as in Fig.2. When the assumption for $\lambda_{max}(\xi)$ holds, it is called “the diffusion driven instability” or “Turing Instability”.

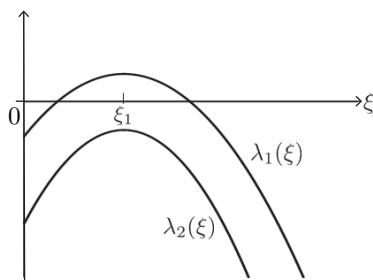


Figure 2: Schematic graphs of $\lambda_1(\xi)$ and $\lambda_2(\xi)$. In this case, $\lambda_{\max}(\xi) = \lambda_1(\xi)$ holds.

Recently, Kondo [8] suggested that the activator-inhibitor system is equivalent to a kernel-based model with the Mexican hat kernel which is a function defined by regarding locally positive and spreading negative parts as a local activation and a lateral inhibition, respectively as in Fig.3 for $x \in \mathbf{R}$ or $\mathbf{x} \in \mathbf{R}^2$. Kondo proposed the following model with convolution (for the definition, see Section 2) by using an integral kernel K

$$u_t = \chi(K * u) - \alpha u, \quad (1.4)$$

where $\chi(r) := \begin{cases} 0, & r \leq 0, \\ r, & 0 < r \leq r^*, \\ r^*, & r \geq r^* \end{cases}$ for a positive constant r^* and the integral kernel function

$K = K(|\mathbf{x}|)$ is a radially symmetric function with Mexican hat profiles or other general functions. The Mexican hat shaped kernel K was given in [8] as the sum of two Gaussian functions

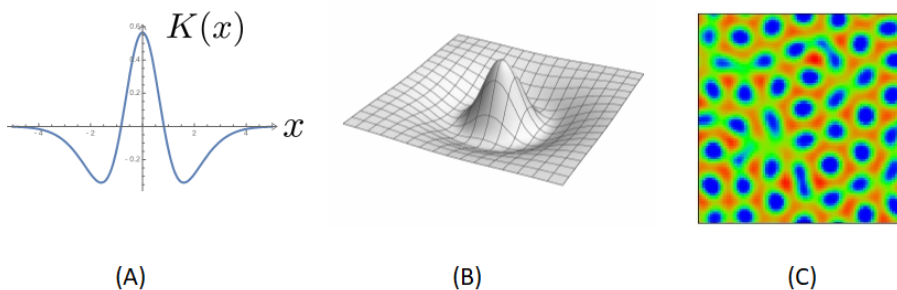


Figure 3: Integral kernels K with the Mexican hat profile. (A) is on \mathbf{R} , (B) is on \mathbf{R}^2 , (C) is the numerically generated 2D patterns with Mexican hat kernel of (B).

and numerically showed the self-organization of spatially periodic 2D patterns similar to those appearing in the activator-inhibitor reaction diffusion systems can be reproduced in (1.4). In practice, the Fourier transformation of the kernel leads the dispersion relation of (1.4) and the existence of a unstable nonzero wave number is easily checked, that is, it has a similar structure of Turing Instability. In that sense, the kernel-based model like (1.4) is called “Kernel-based Turing model (KT model)” in Kondo ([8]).

KT models in the type of (1.4) are very effective to investigate spatially appearing patterns. One reason is that we do not need to know underlying mechanisms of molecules or cells in detail

and that the kernel shape is detected directly from an experimental observation as stated in Kondo [8]. In fact, Kuffler [10] detected the kernel shape related to mammalian retina directly from the observation in real experiments. For example, the diffusion process is phenomenologically expressed by a unimodal localized profile of the kernel with one peak at the center as in Fig.4(A), whose relation was rigorously proved in Bates et. al. [2, 3], and the cell projection which releases the signal molecule at the specific position is by a kernel of a profile with peaks l distant from the center as in Fig.4(B).

Another reason is that KT models can easily reproduce more complicated patterns which are difficult to show by conventional two component reaction diffusion systems such as nested patterns appearing often on animal skins and sea shells. Such complicated patterns were numerically demonstrated in [8] by using several other types of kernel functions. Thus, spatial patterns and

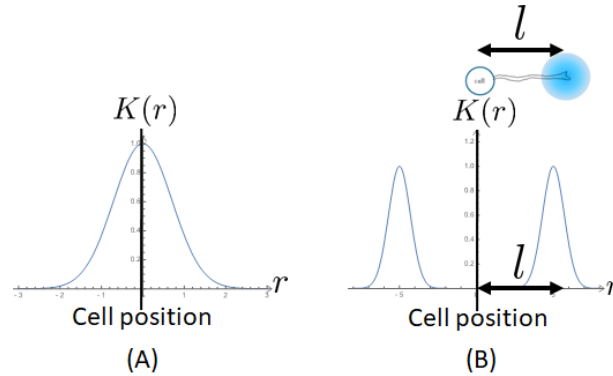


Figure 4: Examples of kernel shapes. (A) corresponds to diffusion process with the peak at the center ($r = 0$). (B) is the kernel shape by cell projections with peaks l distant from the center.

kernel shapes are directly related while kernel shapes are related to the background mechanisms of molecular or cellular processes together with the signal or metabolic networks. It means the possibility of two step approach toward the theoretical understanding of spatial patterns, that is, one is the research into the relation between patterns and kernel shapes which corresponds to the macroscopic researches, another is between kernel shapes and underlying biological mechanisms which corresponds to microscopic ones. Thus, KT models can connect macroscopic structures and microscopic ones through the kernels and this two step approach has a big advantage because these two steps can be treated independently and separately.

Model equations of the type of (1.4) have been proposed in many fields such as neural system (e.g. Amari[1], Murray[13]), cell-cell adhesion problem (e.g. Carrillo et. al.[5], Painter et. al.[18]), Optical illusion (Sushida et. al. [19]). Recently, integral kernels were also used to the development of the continuous method for spatially discrete models ([6]).

In all of them, appropriate integral kernels were adopted from the phenomenological point of view such as the direct detection from the experiments (e.g. Kuffler[10]). In that sense, they can be regarded as works in the step for the relation between patterns and kernel shapes. On the other hand, there have been almost no works in the step between kernel shapes and underlying biological mechanisms while both steps are absolutely necessary to understand the whole mechanism from micro to macro structures.

In this paper, we consider the relation between kernel shapes and the local networks of

metabolites or signals as underlying microscopic mechanisms, and propose a new method to derive an effective kernel shape from an arbitrarily given network. Since the spatial and temporal patterns are essentially governed by the effective equation with the effective kernel, it can give us a unified aspect through the derived effective kernel between seemingly different network systems. Actually, we can identify seemingly different network systems when the effective equations are same.

As one typical example of our approach, let us consider the activator-inhibitor system with the local network like Fig.1, which is basically described by the reaction diffusion system (1.1). As stated in Meinhardt and Gierer ([7]), the essential effect of this system is the property of “local activation with long-range inhibition (LALI)” and it has been believed that the corresponding kernel shape is the Mexican hat profile as in Fig.3. But there have been no theoretical investigation between the kernel shape of the Mexican hat profile and the activator-inhibitor system (1.1). By applying our technique, we systematically derive the Mexican hat shaped kernel from (1.2). The details are shown in Section 3 together with the basic idea of this technique.

We also demonstrate our technique in Section 5 by applying to models with complicated networks including 3 components models in [14], pigment patterns on skins with projections in [15] and regulating waves of differentiation in [20].

For the convenience of readers, we summarize notations and results of the Fourier transformation in Section 2.

2. Preliminaries of the Fourier transformation

In this section, we give several notations and definitions for the Fourier transformation as follows:

For a function $f(x)$ on \mathbf{R} , the Fourier transformation of f is defined by

$$\hat{f}(\xi) = (\mathcal{F}f)(\xi) := \int_{-\infty}^{\infty} f(x)e^{-ix\xi} dx$$

and the inverse Fourier transformation is

$$\check{f}(x) = (\mathcal{F}^{-1}f)(x) := \frac{1}{2\pi} \int_{-\infty}^{\infty} f(\xi)e^{i\xi x} d\xi.$$

In particular,

$$(\mathcal{F}^{-1}f)(x) = \frac{1}{\pi} \int_0^{\infty} f(\xi^2) \cos \xi x d\xi \quad (2.1)$$

holds for $f = f(\xi^2)$. The convolution of f and g is defined by

$$(f * g)(x) := \int_{-\infty}^{\infty} f(x-y)g(y)dy = \int_{-\infty}^{\infty} f(y)g(x-y)dy$$

and $\widehat{f * g} = \hat{f} \cdot \hat{g}$ holds.

For a function $f(x, y)$ on \mathbf{R}^2 , the Fourier transformation is defined by

$$\hat{f}(\xi, \eta) = (\mathcal{F}f)(\xi, \eta) := \int_{-\infty}^{\infty} \int_{-\infty}^{\infty} f(x, y)e^{-i(x\xi + y\eta)} dx dy$$

and the inverse Fourier transformation is

$$\check{f}(x, y) = (\mathcal{F}^{-1}f)(x, y) := \frac{1}{(2\pi)^2} \int_{-\infty}^{\infty} \int_{-\infty}^{\infty} f(\xi, \eta) e^{i(\xi x + \eta y)} d\xi d\eta.$$

The convolution of f and g is

$$(f * g)(x, y) := \int_{-\infty}^{\infty} \int_{-\infty}^{\infty} f(x - x', y - y') g(x', y') dx' dy'$$

and $\widehat{f * g} = \hat{f} \cdot \hat{g}$ holds.

In particular, for a radially symmetric function $K = K(r)$ with $r := \sqrt{x^2 + y^2}$, the Fourier transformation of K is computed by polar coordinate

$$\begin{aligned} \hat{K}(\xi, \eta) &= \int_{-\infty}^{\infty} \int_{-\infty}^{\infty} K(\sqrt{x^2 + y^2}) e^{-i(\xi x + \eta y)} dx dy \\ &= \int_0^{\infty} \int_0^{2\pi} rK(r) e^{-ir(\xi \cos \theta + \eta \sin \theta)} dr d\theta \\ &= \int_0^{\infty} \int_0^{2\pi} rK(r) e^{-irR \cos(\theta - \alpha)} dr d\theta \\ &= \int_0^{\infty} \int_0^{2\pi} rK(r) e^{-irR \cos \theta} dr d\theta, \end{aligned}$$

where $R := \sqrt{\xi^2 + \eta^2}$ and $\alpha = \alpha(\xi, \eta)$. That is, \hat{K} is also radially symmetric and computed as

$$\begin{aligned} \hat{K}(R) &= \int_0^{\infty} \int_0^{2\pi} rK(r) e^{-irR \cos \theta} dr d\theta \\ &= 2 \int_0^{\infty} \int_0^{\pi} rK(r) \cos(rR \sin \theta) d\theta dr \\ &= 4 \int_0^{\infty} \int_0^{\pi/2} rK(r) \cos(rR \sin \theta) d\theta dr. \end{aligned} \tag{2.2}$$

Similarly, the inverse Fourier transformation for a radially symmetric function $K(R)$ is

$$\begin{aligned} \check{K}(r) &= \frac{1}{(2\pi)^2} \int_0^{\infty} \int_0^{2\pi} RK(R) e^{irR \cos \theta} dR d\theta \\ &= \frac{1}{2\pi^2} \int_0^{\infty} \int_0^{\pi} RK(R) \cos(rR \sin \theta) d\theta dR \\ &= \frac{1}{\pi^2} \int_0^{\infty} \int_0^{\pi/2} RK(R) \cos(rR \sin \theta) d\theta dR. \end{aligned} \tag{2.3}$$

Here we give approximations of Dirac δ function, say $\delta(x)$. In general, the following proposition holds.

Proposition 2.1. (Approximation of $\delta(x)$)

Suppose $G_\varepsilon(x)$ is a function satisfying

1) $G_\varepsilon(x) \geq 0$,

2) $\int_{\mathbf{R}} G_\varepsilon(x) dx = 1$,

3) $\lim_{\varepsilon \downarrow 0} \int_{|x| > \eta} G_\varepsilon(x) dx = 0$ for any $\eta > 0$.

Then $(G_\varepsilon * u)(x) \rightarrow u(x)$ as $\varepsilon \downarrow 0$ holds, that is, $G_\varepsilon \rightarrow \delta(x)$.

Typical examples of G_ε are the heat kernel $H_\varepsilon(x) := \frac{1}{\sqrt{4\pi\varepsilon}}e^{-\frac{x^2}{4\varepsilon}}$, and a mollifier $J_\varepsilon(\xi)$ given by $J_\varepsilon(x) := \frac{1}{\varepsilon}J(\frac{x}{\varepsilon})$ for a function $J(x)$ satisfying $J(x) \geq 0$, $\int_{\mathbf{R}} J(x)dx = 1$ and $J(x) = 0$ for $|x| \geq 1$. In this paper, we furthermore impose the condition $\widehat{J}(\xi) \geq 0$ in order to keep the order of eigenvalues while the condition is not required in general. Such a function $J(x)$ is for example made by $J(x) = \{j * j\}(x)$ for a function $j(x)$. Then $\widehat{J}(\xi) = \{\widehat{j}(\xi)\}^2 \geq 0$ holds while $\widehat{H}_\varepsilon(\xi) = e^{-\varepsilon\xi^2} > 0$ holds. Since the mollifier $J_\varepsilon(x)$ satisfies $(J_\varepsilon * u)(x) = 0$ outside of ε -neighborhood of the support of $u(x)$, that is, $\text{supp}(J_\varepsilon * u) \subset W_\varepsilon(\text{supp}(u))$ holds for $W_\varepsilon(\text{supp}(u)) := \{x+y; x \in \text{supp}(u), |y| \leq \varepsilon\}$, it is useful when the support should be taken into account. Above properties for $\delta(x)$ will be used to compute several kernels in the following sections.

In the last of this section, we give several properties of the Lambert W function, say $w = W(z)$, which is a root w of the equation

$$we^w = z. \quad (2.4)$$

Then we have:

Proposition 2.2.

- 1) For $z \geq 0$, (2.4) has a non-negative root $w_0(z) \geq 0$ and any other root w satisfies $\text{Re}(w) < 0$.
- 2) For $-1/e < z < 0$, (2.4) has two real roots $w_1(z), w_2(z)$ ($0 > w_1(z) > -1 > w_2(z)$) and any other root w satisfies $\text{Re}(w) < w_1(z)$.
- 3) For $z = -1/e$, (2.4) has the root $w_0 = -1$ and any other root w satisfies $\text{Re}(w) < -1$.

This proposition is referred to [4]. Here we express the principal branch of the Lambert W function by $W_0(z)$, which is given by $W_0(z) = w_0 \in \mathbf{C}$ satisfying $\text{Re}(w_0) = \max\{\text{Re}(w); we^w = z\}$. It is noted by Proposition 2.2 that $W_0(z)$ is real for $z \geq -1/e$ satisfying $W_0(z) = w_0(z)$ for $z \geq 0$ in 1), $W_0(z) = w_1(z)$ for $-1/e < z < 0$ in 2) and $W_0(-1/e) = -1$ in 3) of Proposition 2.2.

3. The basic idea and the theoretical derivation of the Mexican hat type kernel

In this section, we show our basic idea by using the activator-inhibitor system (1.2) (Fig.5) and theoretically derive the Mexican hat type kernel from it. For simplicity, we consider it on \mathbf{R} .

The activator-inhibitor system has been represented by reaction diffusion systems, which have the following form in a linearized sense

$$\begin{cases} u_t &= d_1 u_{xx} + c_1 u - c_2 v, \\ v_t &= d_2 v_{xx} + c_3 u - c_4 v \end{cases} \quad (3.1)$$

for $x \in \mathbf{R}$, where all coefficients d_1, d_2 and $c_j (j = 1, \dots, 4)$ are positive and $d_1 < d_2$. (3.1) is written in a vector valued form

$$U_t = DU_{xx} + AU, \quad (3.2)$$

where $U = U(t, x) := \begin{pmatrix} u(t, x) \\ v(t, x) \end{pmatrix} \in \mathbf{R}^2$, $D := \text{diag}\{d_1, d_2\} = \begin{pmatrix} d_1 & 0 \\ 0 & d_2 \end{pmatrix}$ and $A := \begin{pmatrix} c_1 & -c_2 \\ c_3 & -c_4 \end{pmatrix}$. Here we note that variables u and v can take any sign since we consider solutions in the neighborhood of an equilibrium by the linearized equation like (3.1).

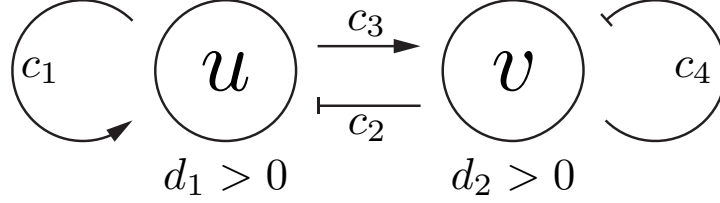


Figure 5: The network of Activator-Inhibitor system. \rightarrow and \perp denote activation and inhibition, respectively.

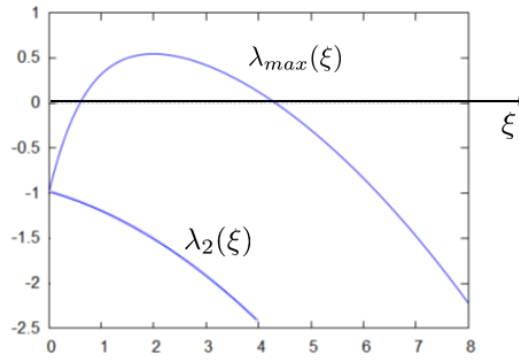


Figure 6: Eigenvalues $\lambda_j(\xi)$ of $B(\xi)$. $c_1 = c_2 = 1$, $c_3 = 4$, $c_4 = 3$, $d_1 = 0.05$ and $d_2 = 3$ in (3.1).

Taking the Fourier transformation of (3.2), we get

$$\widehat{U}_t = B(\xi)\widehat{U}, \quad (3.3)$$

where $B(\xi) := -\xi^2 D + A = \begin{pmatrix} -d_1 \xi^2 + c_1 & -c_2 \\ c_3 & -d_2 \xi^2 - c_4 \end{pmatrix}$. Let $\lambda_j(\xi)$ ($j = 1, 2$) be eigenvalues of $B(\xi)$ and define $\lambda_{\max}(\xi) := \max_j \{\lambda_j(\xi)\}$.

Here we compute the asymptotic profile of $\lambda_{\max}(\xi)$ as $|\xi| \rightarrow \infty$. When $|\lambda_{\max}(\xi) - \lambda_{\pm\infty}(\xi)| \rightarrow 0$ as $\xi \rightarrow \pm\infty$, $\lambda_{\pm\infty}(\xi)$ are called the ‘‘asymptotic profiles of $\lambda_{\max}(\xi)$ ’’ or the ‘‘asymptotic convergence to $\lambda_{\pm\infty}(\xi)$ ’’ as $\xi \rightarrow \pm\infty$, which are expressed by $\lambda_{\max}(\xi) \rightarrow \lambda_{\pm\infty}(\xi)$ as $\xi \rightarrow \pm\infty$. In this example, $\lambda_{\max}(\xi)$ has the asymptotic profile $\lambda_{\max}(\xi) \rightarrow -d_1 \xi^2 + c_1$ as $|\xi| \rightarrow \infty$ by virtue of $d_1 < d_2$ as in Figures 2 and 6. Then we put $\lambda_h(\xi) := -d_1 \xi^2$ (taking the highest order term of ξ) and put $\widehat{U} = e^{i\lambda_h(\xi)} \widehat{V}$. We see that \widehat{V} satisfies

$$\widehat{V}_t = B_h(\xi)\widehat{V}, \quad (3.4)$$

where $B_h(\xi) := B(\xi) - \lambda_h(\xi)I = \begin{pmatrix} c_1 & -c_2 \\ c_3 & -(d_2 - d_1)\xi^2 - c_4 \end{pmatrix}$ and I is the identity matrix. We also divide B_h into $B_h(\xi) = \xi B_1(\xi) + B_0(\xi)$ with $B_0(\xi) = O(1)$ as $|\xi| \rightarrow \infty$, where $B_1(\xi) = \begin{pmatrix} 0 & 0 \\ 0 & -(d_2 - d_1)\xi \end{pmatrix}$ and $B_0(\xi) = \begin{pmatrix} c_1 & -c_2 \\ c_3 & -c_4 \end{pmatrix}$ in this example. Since the Fourier

transformation of the Dirac δ -function is $\widehat{\delta}(\xi) = 1$, we approximate it by the heat kernel $H_\varepsilon(x)$ as in Proposition 2.1 and modify $B_h(\xi)$ as $B_\varepsilon(\xi) := \xi B_1(\xi) + e^{-\varepsilon\xi^2} B_0(\xi)$ for $0 < \varepsilon \ll 1$ by noting $\widehat{H}_\varepsilon(\xi) = e^{-\varepsilon\xi^2}$. We note that this modification is not necessary when $|B_0(\xi)| \rightarrow 0$ as $|\xi| \rightarrow \infty$. By using this modified matrix $B_\varepsilon(\xi)$, we consider

$$\widehat{V}_t = B_\varepsilon(\xi)\widehat{V} \quad (3.5)$$

instead of (3.4).

Now introducing small quantity $0 < \delta \ll 1$, we consider the equation (3.5) at $t + \delta$

$$\widehat{V}_t(t + \delta) = B_\varepsilon(\xi)\widehat{V}(t + \delta). \quad (3.6)$$

Since $\widehat{V}(t) = e^{tB_\varepsilon(\xi)}\widehat{V}_0$ with the initial data \widehat{V}_0 , $\widehat{V}(t + \delta)$ is given by

$$\widehat{V}(t + \delta) = e^{\delta B_\varepsilon(\xi)}\widehat{V}(t).$$

Substituting it into (3.6), we have

$$\widehat{V}_t(t + \delta) = B_\varepsilon(\xi)e^{\delta B_\varepsilon(\xi)}\widehat{V}(t). \quad (3.7)$$

Let $\zeta_j(\xi)$ and $\Phi_j(\xi)$ ($j = 1, 2$) be eigenvalues and the associated eigenvectors of $B_\varepsilon(\xi)$. Since $\widehat{V}(t, \xi)$ is expressed by the linear combination of eigenfunctions of $B_\varepsilon(\xi)$ as $\widehat{V}(t, \xi) = \sum_j \alpha_j(\xi)e^{t\mu_j(\xi)}\Phi_j(\xi)$ for some $\alpha_j(\xi)$ and $\mu_j(\xi) \in \mathbf{C}$, the substitution of it into (3.7) gives

$$\sum_j \alpha_j(\xi)\mu_j(\xi)e^{(t+\delta)\mu_j(\xi)}\Phi_j(\xi) = \sum_j \alpha_j(\xi)B_\varepsilon(\xi)e^{(t+\delta)\mu_j(\xi)B_\varepsilon(\xi)}\Phi_j(\xi), \quad (3.8)$$

which leads

$$\mu_j(\xi)e^{\delta\mu_j(\xi)}\Phi_j(\xi) = \zeta_j(\xi)e^{\delta\zeta_j(\xi)}\Phi_j(\xi)$$

and eventually

$$\mu_j(\xi)e^{\delta\mu_j(\xi)} = \zeta_j(\xi)e^{\delta\zeta_j(\xi)}. \quad (3.9)$$

Note that $\mu_j(\xi) = \zeta_j(\xi)$ is a trivial solution of (3.9) (see e.g. Fig.7) and there are infinite many $\mu_j(\xi)$ satisfying (3.9) for any given $\zeta_j(\xi)$. We need $\mu_j(\xi)$ with maximal real parts among them, that is, we take $\mu_{\max,j}(\xi)$ satisfying $Re(\mu_{\max,j}(\xi)) = \max\{Re(\mu); \mu e^{\delta\mu} = \zeta_j(\xi)e^{\delta\zeta_j(\xi)}\}$, which is known to be real for $\zeta_j(\xi) \in \mathbf{R}$ by Proposition 2.2. Defining $\mu_{\max}(\xi) := \max_j\{\mu_{\max,j}(\xi)\}$, we see $\mu_{\max}(\xi)$ is attained by the principal branch of the Lambert W function as $\mu_{\max}(\xi) = \frac{1}{\delta} \cdot \max_j\{W_0(\delta\zeta_j(\xi)e^{\delta\zeta_j(\xi)})\}$ (see Proposition 2.2). Since $\mu_{\max}(\xi)$ is the most unstable mode, $\widehat{V}(t, \xi)$ of (3.7) satisfies

$$|\widehat{V}(t, \xi) - \alpha(\xi)e^{t\mu_{\max}(\xi)}\Psi(\xi)| \rightarrow 0 \quad (t \rightarrow \infty) \quad (3.10)$$

for almost all initial data $\widehat{V}(0, \xi)$ with some $\alpha(\xi)$ and $\Psi(\xi)$. When (3.10) holds, it is called that $\widehat{V}(t, \xi)$ ‘‘asymptotically converges’’ $\alpha(\xi)e^{t\mu_{\max}(\xi)}\Psi(\xi)$ as $t \rightarrow \infty$. Then we see

$$\widehat{U}(t, \xi) = e^{t\lambda_h(\xi)}\widehat{V}(t, \xi) \rightarrow \alpha(\xi)e^{t(\lambda_h(\xi) + \mu_{\max}(\xi))}\Psi(\xi) \quad (3.11)$$

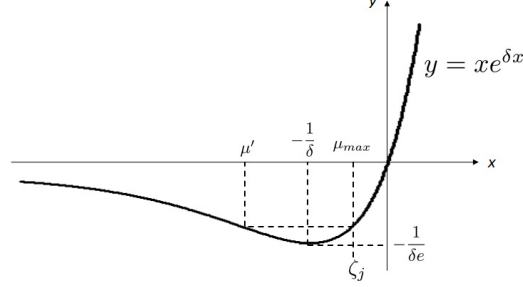


Figure 7: Conceptual figure of solutions μ of (3.9).

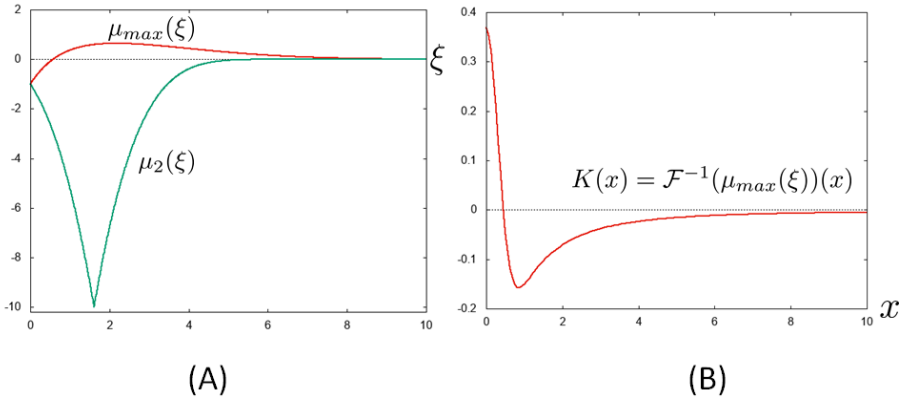


Figure 8: (A) Graph of $\mu_{max}(\xi)$. $\mu_2(\xi)$ denotes the second largest $Re(\mu)$ in (3.9). (B) The derived kernel $K(x) = (\mathcal{F}^{-1} \mu_{max})(x)$. It shows the Mexican hat profile. Parameters are same as those of Fig.6: $c_1 = c_2 = 1$, $c_3 = 4$, $c_4 = 3$, $d_1 = 0.05$ and $d_2 = 3$ in (3.1). ε and δ in (3.6) are taken as $\varepsilon = 0.05$, $\delta = 0.1$. Only the right half pictures are drawn both in (A) and (B).

as $t \rightarrow \infty$. Thus, $\widehat{U}(t)$ satisfies asymptotically $\widehat{U}_t = (\lambda_h(\xi) + \mu_{max}(\xi))\widehat{U}$ and therefore for any element of \widehat{U} , say \widehat{w} , $\widehat{w}_t = (\lambda_h(\xi) + \mu_{max}(\xi))\widehat{w}$ holds. Since $\zeta_j(\xi) \rightarrow 0$ or $-\infty$ as $|\xi| \rightarrow \infty$ by the form of $B_\varepsilon(\xi)$, $\mu_{max}(\xi) \rightarrow 0$ holds as $|\xi| \rightarrow \infty$ and $\mu_{max} \in L^2(\mathbf{R})$ is expected for almost all cases as shown in several applications mentioned in this paper. Thus we obtain the equation of w

$$w_t = d_1 w_{xx} + K * w \quad (3.12)$$

as the effective equation, where we use $\mathcal{F}^{-1}(-d_1 \xi^2) = d_1 \partial_x^2$ and define $K(x) := \mathcal{F}^{-1}(\mu_{max}(\xi))(x)$, the inverse Fourier transformation of the function $\mu_{max}(\xi)$. Fig.8 is a numerical simulation under the indicated parameters. We note that the kernel $K(x)$ gives the Mexican hat type profile. In practical computations, we use

$$w_t = d_1 w_{xx} + \chi(K * w) \quad (3.13)$$

with an appropriate cut-off function $\chi(r)$ as in (1.4).

Remark 3.1. The above matrix $B(\xi)$ and the eigenvalue $\lambda_j(\xi)$ can be written as $B(\xi^2)$ and $\lambda_j(\xi^2)$ from the forms. In general, the matrix and the eigenvalue corresponding to $B(\xi)$ and

$\lambda_j(\xi)$ depend only on ξ^2 when the spatial movement is only by a local diffusion like this example. In this case, one dimensional analysis is enough because the Fourier transformation on 2D just replaces ξ^2 by $\xi^2 + \eta^2$, that is, the matrix $B(\xi^2 + \eta^2)$ and the eigenvalue $\lambda_j(\xi^2 + \eta^2)$ in 2D without any other change, which means the reduced kernel in 1D and 2D are almost same (refer Section 5).

Remark 3.2. The equations (1.4) and (3.13) seem different each other. But they are essentially same in the following sense: The diffusion is approximated by the relation $J_\varepsilon * u = \gamma_0 u + \varepsilon^2 \gamma_1 u_{xx} + O(\varepsilon^4)$ as $\varepsilon \rightarrow +0$, where $J_\varepsilon(x) := \frac{1}{\varepsilon} J(\frac{x}{\varepsilon})$ for an even function $J(x)$ satisfying $J(x) \geq 0$ and $\gamma_0 := \int_{\mathbf{R}} J(x) dx$, $\gamma_1 := \frac{1}{2} \int_{\mathbf{R}} x^2 J(x) dx$ (e.g. [3, 13]). Then the reduced equation (3.12) without cut-off function in (3.13) is expressed as

$$w_t = K' * w - \frac{\gamma_0}{\varepsilon^2 \gamma_1} w + O(\varepsilon^2) \quad (3.14)$$

with $K'(x) := \frac{d_1}{\varepsilon^2 \gamma_1} J_\varepsilon(x) + K(x)$, which is the same form as (1.4) without cut-off function. Thus, (1.4) and (3.13) are essentially same and we are adopting the equations in the form of (3.13) in this paper.

4. Treatment for arbitrary networks

4.1. Basic treatment for general networks - case of real eigenvalues -

In this section, we first give the idea to treat general cases of multiple components, but consider on one dimensional space just for the simplicity. Let $U = {}^t(u_1, \dots, u_N) \in \mathbf{R}^N$ and U is supposed to be described by the equation

$$U_t = \mathbf{J}U + AU, \quad (4.1)$$

where $\mathbf{J}U := {}^t(J_1 * u_1, \dots, J_N * u_N)$ for $\mathbf{J} := {}^t(J_1, \dots, J_N)$ with kernels J_j corresponds to the spatial movement and N -th order square matrix A denotes the local network like the matrix A in (3.2). Taking the Fourier transformation of (4.1), we have

$$\widehat{U}_t = B(\xi) \widehat{U}, \quad (4.2)$$

where $B(\xi) := \widehat{\mathbf{J}} + A$. Let $\lambda_j(\xi)$ ($j = 1, \dots, N$) be eigenvalues of $B(\xi)$. In this subsection, all $\lambda_j(\xi)$ are supposed to be real. Quite similarly to the previous section, we define $\lambda_{\max}(\xi) := \max_j \{\lambda_j(\xi)\}$ and $\lambda_h(\xi)$ be the highest order term in ξ of the asymptotic profile of $\lambda_{\max}(\xi)$ as $|\xi| \rightarrow \infty$. Here we give the precise way to get $\lambda_h(\xi)$. Let $\lambda_{\pm\infty}(\xi)$ be the asymptotic profile of $\lambda_{\max}(\xi)$ satisfying $\lambda_{\max}(\xi) \rightarrow \lambda_{\pm\infty}(\xi)$ as $\xi \rightarrow \pm\infty$. When $|\lambda_{\pm\infty}(\xi)| \rightarrow \infty$ as $\xi \rightarrow \pm\infty$ and the highest order terms of $\lambda_{\pm\infty}(\xi)$ are coincident each other, take the same highest order term of $\lambda_{\pm\infty}(\xi)$ as $\lambda_h(\xi)$ and when $\lambda_{\pm\infty}(\xi) \rightarrow O(1)$, take $\lambda_h(\xi) = 0$. For example, when $\lambda_{\pm\infty}(\xi)$ is given by $\lambda_{\pm\infty}(\xi) = a_1 \xi^2 + a_{\pm 2} \xi + a_{\pm 3}$ for $a_j \in \mathbf{C}$ and $a_1 \neq 0$, we put $\lambda_h(\xi) = a_1 \xi^2$ and when $\lambda_{\pm\infty}(\xi) = a_{\pm 3}$, we put $\lambda_h(\xi) = 0$.

Transforming $\widehat{U}(t) = e^{t\lambda_h(\xi)}\widehat{V}(t)$, we have the equation of \widehat{V}

$$\widehat{V}_t = B_h(\xi)\widehat{V} \quad (4.3)$$

with $B_h(\xi) := \{B(\xi) - \lambda_h(\xi)I\}$. Expressing $B_h(\xi)$ in the form $B_h(\xi) = \xi B_1(\xi) + B_0(\xi)$ with $B_0(\xi) = O(1)$ as $|\xi| \rightarrow \infty$, we define $B_\varepsilon(\xi) := \xi B_1(\xi) + e^{-\varepsilon\xi^2}B_0(\xi)$ and consider the equation

$$\widehat{V}_t = B_\varepsilon(\xi)\widehat{V} \quad (4.4)$$

instead of (4.3). Let $\zeta_j(\xi)$ and $\Phi_j(\xi)$ ($j = 1, \dots, N$) be eigenvalues and the associated eigenvectors of $B_\varepsilon(\xi)$, which are supposed to be real in this subsection.

Taking the time $t + \delta$ for $0 < \delta \ll 1$ in (4.4), we see

$$\widehat{V}_t(t + \delta) = B_\varepsilon(\xi)\widehat{V}(t + \delta) \quad (4.5)$$

and therefore

$$\widehat{V}_t(t + \delta) = B_\varepsilon(\xi)e^{\delta B_\varepsilon(\xi)}\widehat{V}(t) \quad (4.6)$$

from (4.4). Then we express $\widehat{V}(t, \xi) = \sum_j \alpha_j(\xi)e^{t\mu_j(\xi)}\Phi_j(\xi)$ and the substitution of it into (4.6)

leads

$$\mu_j(\xi)e^{\delta\mu_j(\xi)} = \zeta_j(\xi)e^{\delta\zeta_j(\xi)} \quad (4.7)$$

in quite a similar manner to (3.8) and (3.9). Define $\mu_{\max}(\xi)$ as the value satisfying

$$Re(\mu_{\max}(\xi)) = \max_j \{Re(\mu); \mu e^{\delta\mu} = \zeta_j(\xi)e^{\delta\zeta_j(\xi)}, j = 1, 2, \dots, N\}$$

similarly to Section 3, which is given by $\mu_{\max}(\xi) = \max_j \{1/\delta \cdot W_0(\delta\zeta_j(\xi)e^{\delta\zeta_j(\xi)})\}$ when $\zeta_j(\xi) \in \mathbf{R}$ by Proposition 2.2.

Remark 4.1. $\mu_j(\xi) = \zeta_j(\xi)$ holds when $\zeta_j(\xi) > -\frac{1}{\delta}$ (see Figure 7).

Since $\mu_{\max}(\xi)$ is the most unstable eigenvalue for $\xi \in \mathbf{R}$, we can expect $\widehat{V}(t)$ of (4.6) asymptotically converges $\widehat{V}(t, \xi) \rightarrow \alpha(\xi)e^{t\mu_{\max}(\xi)}\Phi(\xi)$ ($t \rightarrow \infty$) with some $\alpha(\xi)$ and $\Phi(\xi)$ for almost all initial data and hence

$$\widehat{U}(t, \xi) = e^{t\lambda_h(\xi)}\widehat{V}(t, \xi) \rightarrow \alpha(\xi)e^{t(\lambda_h(\xi) + \mu_{\max}(\xi))}\Phi(\xi) \quad (4.8)$$

as $t \rightarrow \infty$. Thus, $\widehat{U}(t)$ satisfies asymptotically $\widehat{U}_t = (\lambda_h(\xi) + \mu_{\max}(\xi))\widehat{U}$ and therefore for any element of \widehat{U} , say \widehat{w} , $\widehat{w}_t = (\lambda_h(\xi) + \mu_{\max}(\xi))\widehat{w}$ holds. Consequently we obtain the equation of w

$$w_t = \mathcal{L}w + K * w \quad (4.9)$$

as the effective equation, where $K(x) := \mathcal{F}^{-1}(\mu_{\max}(\xi))$ and $\mathcal{L} := \mathcal{F}^{-1}(\lambda_h(\xi))$, which is treated as a differential operator such as $\mathcal{F}^{-1}(-\xi^2) = \partial_x^2$. Here we note that $\mu_{\max}(\xi) \rightarrow 0$ as $|\xi| \rightarrow \infty$ because $\zeta_j(\xi) \rightarrow 0$ or $-\infty$.

This is the basic idea in the case that all $\lambda_j(\xi)$ are real valued and there exists only one maximal eigenvalue for each ξ . But this is a specially simple case because there can be several other cases. In the following subsection, the case that $B(\xi)$ have complex eigenvalues on some range of $\xi \in \mathbf{R}$ is considered.

4.2. Basic treatment for general networks

- case of complex eigenvalues -

In this section, we consider the case that $B(\xi)$ in (4.2) have complex eigenvalues for an interval of ξ . We define $\lambda_{max}(\xi) := \max_j \{Re(\lambda_j(\xi))\}$ and the asymptotic profile $\lambda_\infty(\xi)$ of $\lambda_{max}(\xi)$ by $\lambda_{max}(\xi) \rightarrow \lambda_\infty(\xi)$ as $|\xi| \rightarrow \infty$. First, we assume

$$\lambda_j(\xi) - \lambda_\infty(\xi) \rightarrow 0 \quad (|\xi| \rightarrow \infty). \quad (4.10)$$

Let $\lambda_h(\xi)$ be the highest order term of $\lambda_\infty(\xi)$ and $B_h(\xi) := B(\xi) - \lambda_h(\xi)I$. As in the previous section, we divide $B_h(\xi)$ as $B_h(\xi) = \xi B_1(\xi) + B_0(\xi)$ with $B_0(\xi) = O(1)$ and define $B_\varepsilon(\xi) = \xi B_1(\xi) + e^{-\varepsilon \xi^2} B_0(\xi)$.

Let $\zeta_j(\xi)$ and $\Phi_j(\xi)$ be eigenvalues and the associated eigenvectors of $B_\varepsilon(\xi)$ and consider the equation (4.6) together with (4.7) in the case of complex eigenvalues. Define

$$\mu_{max}(\xi) := \max_j \{Re(\mu); \mu e^{\delta \mu} = \zeta_j(\xi) e^{\delta \zeta_j(\xi)}, j = 1, 2, \dots, N\}$$

and assume that $\zeta_1(\xi), \zeta_2(\xi)$ satisfy the following three assumptions (H1), (H2) and (H3).

(H1): $\mu_{max}(\xi)$ is attained by $\zeta_1(\xi)$, that is, $\mu_{max}(\xi) = \max\{Re(\mu); \mu e^{\delta \mu} = \zeta_1(\xi) e^{\delta \zeta_1(\xi)}\}$.

(H2): There exists ξ_c such that $\zeta_1(\xi) > \zeta_2(\xi)$ for $\xi < \xi_c$, $\zeta_1(\xi_c) = \zeta_2(\xi_c) \in \mathbf{R}$ and $\zeta_1(\xi) = \overline{\zeta_2(\xi)} = a(\xi) + ib(\xi)$ for $\xi > \xi_c$ with $a(\xi) \in \mathbf{R}$ and $b(\xi) > 0$ satisfying $a(\xi_c) = \zeta_1(\xi_c) = \zeta_2(\xi_c)$ and $b(\xi_c) = 0$. Moreover, $\Phi_1(\xi_c) = \Phi_2(\xi_c)$ holds.

(H3): Define $\Psi(\xi) := \frac{\Phi_2(\xi) - \Phi_1(\xi)}{\zeta_2(\xi) - \zeta_1(\xi)}$. Then, there exists a limit $\lim_{\xi \rightarrow \xi_c} \Psi(\xi)$.

Remark 4.2. It follows that $b(\xi) \rightarrow 0$ as $|\xi| \rightarrow \infty$ by (4.10) and also that $\Psi(\xi)$ is a continuous real vector-valued function on the whole line \mathbf{R} by the definition in (H3).

Substituting $\Phi_2(\xi) = \Phi_1(\xi) + \{\zeta_2(\xi) - \zeta_1(\xi)\}\Psi(\xi)$ into $B_\varepsilon(\xi)\Phi_2(\xi) = \zeta_2(\xi)\Phi_2(\xi)$ for $\xi < \xi_c$, we have $\zeta_1(\xi)\Phi_1(\xi) + \{\zeta_2(\xi) - \zeta_1(\xi)\}B_\varepsilon(\xi)\Psi(\xi) = \zeta_2(\xi)\Phi_1(\xi) + \zeta_2(\xi)\{\zeta_2(\xi) - \zeta_1(\xi)\}B_\varepsilon(\xi)\Psi(\xi)$ and consequently $\{B_\varepsilon(\xi) - \zeta_2(\xi)I\}\tilde{\Phi}(\xi) = \Phi_1(\xi)$. That is,

$$\begin{cases} \{B_\varepsilon(\xi) - \zeta_1(\xi)I\}\Phi_1(\xi) & = 0, \\ \{B_\varepsilon(\xi) - \zeta_2(\xi)I\}\Psi(\xi) & = \Phi_1(\xi) \end{cases} \quad (4.11)$$

holds for $\xi < \xi_c$.

On the other hand, we have for $\xi > \xi_c$,

$$\begin{cases} \{B_\varepsilon(\xi) - a(\xi)I\}\mathbf{p}(\xi) & = -b(\xi)\mathbf{q}(\xi), \\ \{B_\varepsilon(\xi) - a(\xi)I\}\mathbf{q}(\xi) & = b(\xi)\mathbf{p}(\xi) \end{cases}$$

when we express $\Phi_1(\xi) = \mathbf{p}(\xi) + i\mathbf{q}(\xi) = \overline{\Phi_2(\xi)}$ with $\mathbf{p}(\xi), \mathbf{q}(\xi) \in \mathbf{R}^N$. Since the definition of $\Psi(\xi)$ leads $\mathbf{q}(\xi) = b(\xi)\Psi(\xi)$ and consequently

$$\begin{cases} \{B_\varepsilon(\xi) - a(\xi)I\}\mathbf{p}(\xi) & = -b^2(\xi)\Psi(\xi), \\ \{B_\varepsilon(\xi) - a(\xi)I\}\Psi(\xi) & = \mathbf{p}(\xi) \end{cases} \quad (4.12)$$

for $\xi > \xi_c$. (4.11) and (4.12) imply that the functions $b(\xi)$, $\zeta_j(\xi)$ ($j = 1, 2$) and the vector $\Phi_1(\xi)$ can be extended as real valued continuous functions and a vector on the whole line \mathbf{R} by

$$b(\xi) := \begin{cases} 0 & (\xi \leq \xi_c) \\ b(\xi) & (\xi > \xi_c) \end{cases}, \quad \omega_j(\xi) := \begin{cases} \zeta_j(\xi) & (\xi \leq \xi_c) \\ a(\xi) & (\xi > \xi_c) \end{cases}, \quad \Psi_1(\xi) := \begin{cases} \Phi_1(\xi) & (\xi \leq \xi_c) \\ \mathbf{p}(\xi) & (\xi > \xi_c) \end{cases}. \quad (4.13)$$

Thus (4.11) and (4.12) are unified as one system on \mathbf{R}

$$\begin{cases} \{B_\varepsilon(\xi) - \omega_1(\xi)I\}\Psi_1(\xi) &= -b^2(\xi)\Psi, \\ \{B_\varepsilon(\xi) - \omega_2(\xi)I\}\Psi(\xi) &= \Psi_1(\xi). \end{cases} \quad (4.14)$$

Now we go back the equation (4.6) of \widehat{V} . Let the solution \widehat{V} of (4.6) be of the form $\alpha\Psi_1(\xi) + \beta\Psi(\xi)$ for $\alpha, \beta \in \mathbf{R}$. Since (4.14) shows

$$B_\varepsilon(\xi)(\alpha\Psi_1(\xi) + \beta\Psi(\xi)) = (\omega_1(\xi)\alpha + \beta)\Psi_1(\xi) + (-b^2(\xi)\alpha + \omega_2(\xi)\beta)\Psi(\xi),$$

(4.6) becomes the equation of α and β as

$$\frac{d}{dt} \begin{pmatrix} \alpha(t+\delta) \\ \beta(t+\delta) \end{pmatrix} = \widetilde{B}_\varepsilon(\xi) e^{\delta \widetilde{B}_\varepsilon(\xi)} \begin{pmatrix} \alpha(t) \\ \beta(t) \end{pmatrix}, \quad (4.15)$$

where $\widetilde{B}_\varepsilon(\xi) := \begin{pmatrix} \omega_1(\xi) & 1 \\ -b^2(\xi) & \omega_2(\xi) \end{pmatrix}$. Since the eigenvalues of $\widetilde{B}_\varepsilon(\xi)$ are $\widetilde{\omega}_1(\xi) := \omega_1(\xi) + ib(\xi)$ and $\widetilde{\omega}_2(\xi) := \omega_2(\xi) - ib(\xi)$ with associated eigenvectors $\widetilde{\Psi}_1(\xi) = {}^t(1, ib(\xi))$ and $\widetilde{\Psi}_2(\xi) = {}^t(1, \omega_2(\xi) - \omega_1(\xi) - ib(\xi))$ respectively, $\begin{pmatrix} \alpha \\ \beta \end{pmatrix} = e^{t\mu} \widetilde{\Psi}$ with (4.15) leads

$$\mu e^{\delta\mu} = \widetilde{\omega}_j e^{\delta\widetilde{\omega}_j} = e^{\delta\omega_j} \{(\omega_j \cos \delta b - b \sin \delta b) \pm i(b \cos \delta b + \omega_j \sin \delta b)\} \quad (4.16)$$

by taking $\widetilde{\Psi} = \widetilde{\Psi}_j(\xi)$. Let the set $\widetilde{\mathcal{M}}_j(\xi) := \{\mu; \mu e^{\delta\mu} = \widetilde{\omega}_j e^{\delta\widetilde{\omega}_j}\}$ and define $\widetilde{\mu}_j(\xi) \in \widetilde{\mathcal{M}}_j(\xi)$ for $j = 1, 2$ such that $Re(\widetilde{\mu}_j(\xi)) = \max\{Re(\mu); \mu \in \widetilde{\mathcal{M}}_j(\xi)\}$. Here we note that these $\widetilde{\mu}_j(\xi)$ give $\mu_{max}(\xi)$, that is, $\mu_{max}(\xi) = \max_{j=1,2} \{Re(\widetilde{\mu}_j(\xi))\}$. Then we can take the solution $\begin{pmatrix} \alpha \\ \beta \end{pmatrix}$ of (4.15) by $\begin{pmatrix} \alpha(t) \\ \beta(t) \end{pmatrix} = e^{t\widetilde{\mu}_1} \widetilde{\Psi}_1 + e^{t\widetilde{\mu}_2} \widetilde{\Psi}_2$, which leads the equation of $\alpha(t)$ and $\beta(t)$ as

$$\begin{aligned} \frac{d}{dt} \begin{pmatrix} \alpha \\ \beta \end{pmatrix} &= [\widetilde{\Psi}_1, \widetilde{\Psi}_2] \begin{pmatrix} \widetilde{\mu}_1 & 0 \\ 0 & \widetilde{\mu}_2 \end{pmatrix} [\widetilde{\Psi}_1, \widetilde{\Psi}_2]^{-1} \begin{pmatrix} \alpha \\ \beta \end{pmatrix} \\ &= \frac{1}{\omega_2 - \omega_1 - 2ib} \begin{pmatrix} (\omega_2 - \omega_1)\widetilde{\mu}_1 - ib(\widetilde{\mu}_1 + \widetilde{\mu}_2) & -\widetilde{\mu}_1 + \widetilde{\mu}_2 \\ ib(\omega_2 - \omega_1 - ib)(\widetilde{\mu}_1 - \widetilde{\mu}_2) & (\omega_2 - \omega_1)\widetilde{\mu}_2 - ib(\widetilde{\mu}_1 + \widetilde{\mu}_2) \end{pmatrix} \begin{pmatrix} \alpha \\ \beta \end{pmatrix}. \end{aligned} \quad (4.17)$$

By the way of construction in (4.13), we see $\widetilde{\omega}_1(\xi) \neq \widetilde{\omega}_2(\xi)$ and $\widetilde{\omega}_j(\xi) = \zeta_j(\xi) \in \mathbf{R}$ for $\xi < \xi_c$, $\widetilde{\omega}_1(\xi_c) = \widetilde{\omega}_2(\xi_c)$, $\widetilde{\omega}_1(\xi) = \widetilde{\omega}_2(\xi)$ for $\xi > \xi_c$, we can also assume $\widetilde{\mu}_1(\xi) \neq \widetilde{\mu}_2(\xi)$ and $\widetilde{\mu}_j(\xi) \in \mathbf{R}$ for $\xi < \xi_c$, $\widetilde{\mu}_1(\xi_c) = \widetilde{\mu}_2(\xi_c)$, $\widetilde{\mu}_1(\xi) = \widetilde{\mu}_2(\xi)$ for $\xi > \xi_c$. Then, (4.17) becomes

$$\frac{d}{dt} \begin{pmatrix} \alpha \\ \beta \end{pmatrix} = \frac{1}{\zeta_2 - \zeta_1} \begin{pmatrix} (\zeta_2 - \zeta_1)\widetilde{\mu}_1 & -\widetilde{\mu}_1 + \widetilde{\mu}_2 \\ 0 & (\zeta_2 - \zeta_1)\widetilde{\mu}_2 \end{pmatrix} \begin{pmatrix} \alpha \\ \beta \end{pmatrix} = \begin{pmatrix} \widetilde{\mu}_1 & \frac{\widetilde{\mu}_2 - \widetilde{\mu}_1}{\omega_2 - \omega_1} \\ 0 & \widetilde{\mu}_2 \end{pmatrix} \begin{pmatrix} \alpha \\ \beta \end{pmatrix} \quad (4.18)$$

for $\xi < \xi_c$ and

$$\frac{d}{dt} \begin{pmatrix} \alpha \\ \beta \end{pmatrix} = \frac{1}{-2ib} \begin{pmatrix} -ib(\tilde{\mu}_1 + \tilde{\mu}_2) & -\tilde{\mu}_1 + \tilde{\mu}_2 \\ b^2(\tilde{\mu}_1 - \tilde{\mu}_2) & -ib(\tilde{\mu}_1 + \tilde{\mu}_2) \end{pmatrix} \begin{pmatrix} \alpha \\ \beta \end{pmatrix} = \begin{pmatrix} \tilde{a} & \tilde{b}/b \\ -\tilde{b}b & \tilde{a} \end{pmatrix} \begin{pmatrix} \alpha \\ \beta \end{pmatrix} \quad (4.19)$$

for $\xi > \xi_c$, where $\tilde{\mu}_1(\xi) = \overline{\tilde{\mu}_2(\xi)} = \tilde{a}(\xi) + i\tilde{b}(\xi)$ for $\xi > \xi_c$. Therefore, if the limit exists and

$$\lim_{\xi \rightarrow \xi_c - 0} \frac{\tilde{\mu}_2(\xi) - \tilde{\mu}_1(\xi)}{\tilde{\zeta}_2(\xi) - \tilde{\zeta}_1(\xi)} = \lim_{\xi \rightarrow \xi_c + 0} \frac{\tilde{b}(\xi)}{b(\xi)} =: \tilde{p}_c$$

holds, then we can define real valued continuous functions on \mathbf{R} by

$$\tilde{p}(\xi) := \begin{cases} \frac{\tilde{\mu}_2(\xi) - \tilde{\mu}_1(\xi)}{\tilde{\zeta}_2(\xi) - \tilde{\zeta}_1(\xi)} & (\xi < \xi_c) \\ \tilde{p}_c & (\xi = \xi_c) \\ \frac{\tilde{b}(\xi)}{b(\xi)} & (\xi > \xi_c) \end{cases}, \quad \tilde{v}_j(\xi) := \begin{cases} \tilde{\mu}_j(\xi) & (\xi \leq \xi_c) \\ \tilde{a}(\xi) & (\xi > \xi_c) \end{cases}, \quad \tilde{q}(\xi) := \begin{cases} 0 & (\xi \leq \xi_c) \\ -\tilde{b}(\xi)b(\xi) & (\xi > \xi_c) \end{cases} \quad (4.20)$$

and equations (4.18) and (4.19) are unified as one equation

$$\frac{d}{dt} \begin{pmatrix} \alpha \\ \beta \end{pmatrix} = \begin{pmatrix} \tilde{v}_1(\xi) & \tilde{p}(\xi) \\ \tilde{q}(\xi) & \tilde{v}_2(\xi) \end{pmatrix} \begin{pmatrix} \alpha \\ \beta \end{pmatrix}. \quad (4.21)$$

Thus we get \hat{V} of (4.6) as $\hat{V} = \alpha\Psi_1 + \beta\Psi$ and $\hat{U} = e^{t\lambda_h}\hat{V} = e^{t\lambda_h}\alpha\Psi_1 + e^{t\lambda_h}\beta\Psi$. This implies that $\hat{U} = \alpha'\Psi_1 + \beta'\Psi$ satisfies

$$\frac{d}{dt} \begin{pmatrix} \alpha' \\ \beta' \end{pmatrix} = \begin{pmatrix} \tilde{v}_1(\xi) + \lambda_h(\xi) & \tilde{p}(\xi) \\ \tilde{q}(\xi) & \tilde{v}_2(\xi) + \lambda_h(\xi) \end{pmatrix} \begin{pmatrix} \alpha' \\ \beta' \end{pmatrix}. \quad (4.22)$$

Consequently, we can get the equation of $X := \mathcal{F}^{-1}\alpha'$, $Y := \mathcal{F}^{-1}\beta'$ as

$$\begin{cases} \dot{X} &= \mathcal{L}X + K * X + L * Y, \\ \dot{Y} &= \mathcal{L}Y + M * X + N * Y, \end{cases} \quad (4.23)$$

where $K(x) := \mathcal{F}^{-1}(\tilde{v}_1(\xi))(x)$, $L(x) := \mathcal{F}^{-1}(\tilde{p}(\xi))(x)$, $M(x) := \mathcal{F}^{-1}(\tilde{q}(\xi))(x)$, $N(x) := \mathcal{F}^{-1}(\tilde{v}_2(\xi))(x)$ and the differential operator $\mathcal{L} := \mathcal{F}^{-1}(\lambda_h(\xi))$.

The simpler case stated in the previous subsection corresponds to the case $Y = 0$ and $M = 0$ in (4.23).

We summarize several cases which can occur in practical situations in the following subsections.

4.3. Practical ways

In practical situations, we will meet several difficulties and complication in calculation. In this section, we give practical ways to obtain effective equations by using approximations.

Hereafter, we assume the asymptotic profile $\lambda_\infty(\xi)$ is real for any $\xi \in \mathbf{R}$.

In order to obtain $\mu_{\max}(\xi)$ in (4.7), (4.16), we give the following two practical ways.

Practical way I):

Define $M_{\max}(z) := \max\{Re(\mu); \mu e^{\delta\mu} = ze^{\delta z}\}$ for a given $z \in \mathbf{C}$. Then $\mu_{\max}(\xi)$ is given by

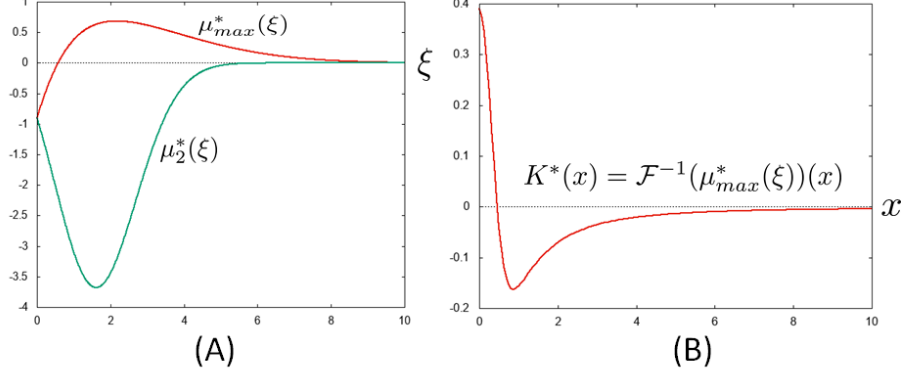


Figure 9: (A) Graph of $\mu_{max}^*(\xi)$. $\mu_2^*(\xi)$ denotes the second largest $M^*(\zeta_j(\xi))$ for the eigenvalues $\zeta_j(\xi) \in B_\varepsilon(\xi)$. (B) The derived kernel $K^*(x) = (\mathcal{F}^{-1}\mu_{max}^*)(x)$, which shows the Mexican hat profile. Parameters are same as those of Fig.6 and Fig.8: $c_1 = c_2 = 1$, $c_3 = 4$, $c_4 = 3$, $d_1 = 0.05$, $d_2 = 3$ and $\varepsilon = 0.05$, $\delta = 0.1$. Only the right half pictures are drawn both in (A) and (B).

$\mu_{max}(\xi) = \max_j \{M_{max}(\zeta_j(\xi)); \zeta_j(\xi) \in \sigma(B_\varepsilon(\xi))\}$. Thus, $\mu_{max}(\xi)$ is calculated by the function $M_{max}(z)$. On the other hand, $M_{max}(z) = \frac{1}{\delta} W_0(\delta z e^{\delta z})$ holds for $z \in \mathbf{R}$ by Proposition 2.2 and the graph of $\frac{1}{\delta} W_0(\delta z e^{\delta z})$ is qualitatively close to $M^*(z) := z e^{\delta z}$ when $z \in \mathbf{R}$. Hence we adopt $M^*(z)$ instead of $M_{max}(z)$ as a rough approximation and use $\mu_{max}^*(\xi) := \max_j \{M^*(\zeta_j(\xi))\}$ as the approximation of $\mu_{max}(\xi)$ when $\zeta_j(\xi) \in \mathbf{R}$. In Fig.9, the kernel $K^*(x) = \mathcal{F}^{-1}(\mu_{max}^*(\xi))(x)$ is drawn under the same parameters as Fig.8. It suggests that the essential structure of the original kernel $K(x)$ is retained by this rough approximation.

When $\zeta_j(\xi)$ is complex satisfying conditions in Section 4.2, we use $\tilde{\mu}_j^*(\xi) := M^*(\tilde{\omega}_j(\xi))$ in (4.16) as the approximation of $\tilde{\mu}_j(\xi)$. Then $\tilde{p}(\xi)$, $\tilde{\mu}_j(\xi)$ and $\tilde{q}(\xi)$ in (4.20) are all calculated as follows:

Since

$$\begin{aligned} \tilde{\mu}_j^*(\xi) &= M^*(\tilde{\omega}_j(\xi)) \\ &= e^{\delta \omega_j(\xi)} \{(\omega_j(\xi) \cos \delta b(\xi) - b(\xi) \sin \delta b(\xi)) \pm i(b(\xi) \cos \delta b(\xi) + \omega_j(\xi) \sin \delta b(\xi))\} \end{aligned}$$

($j = 1, 2$) as in (4.16), we see from (4.13)

$$\tilde{\mu}_j^*(\xi) = \begin{cases} M^*(\zeta_j(\xi)) & (\xi < \xi_c), \\ e^{\delta a(\xi)} \{(a(\xi) \cos \delta b(\xi) - b(\xi) \sin \delta b(\xi)) \pm i(b(\xi) \cos \delta b(\xi) + a(\xi) \sin \delta b(\xi))\} & (\xi > \xi_c) \end{cases}$$

and hence we put for $\xi > \xi_c$

$$\tilde{a}^*(\xi) := e^{\delta a(\xi)} \{a(\xi) \cos \delta b(\xi) - b(\xi) \sin \delta b(\xi)\},$$

$$\tilde{b}^*(\xi) := e^{\delta a(\xi)} \{b(\xi) \cos \delta b(\xi) + a(\xi) \sin \delta b(\xi)\},$$

which leads

$$\tilde{p}^*(\xi) := \begin{cases} \frac{\tilde{\mu}_2^*(\xi) - \tilde{\mu}_1^*(\xi)}{\zeta_2^*(\xi) - \zeta_1^*(\xi)} = \frac{M^*(\zeta_2(\xi)) - M^*(\zeta_1(\xi))}{\zeta_2(\xi) - \zeta_1(\xi)} & (\xi < \xi_c), \\ \tilde{p}_c^* := e^{\delta a(\xi_c)} (1 + \delta a(\xi_c)) & (\xi = \xi_c), \\ \frac{\tilde{b}^*(\xi)}{b(\xi)} = e^{\delta a(\xi)} \{(\cos \delta b(\xi) + a(\xi) \frac{\sin \delta b(\xi)}{b(\xi)})\} & (\xi > \xi_c) \end{cases} \quad (4.24)$$

and

$$\tilde{v}_j^*(\xi) := \begin{cases} \tilde{\mu}_j^*(\xi) = M^*(\zeta_j(\xi)) & (\xi \leq \xi_c), \\ \tilde{a}^*(\xi) & (\xi > \xi_c), \end{cases} \quad (4.25)$$

$$\tilde{q}^*(\xi) := \begin{cases} 0 & (\xi \leq \xi_c), \\ -\tilde{b}^*(\xi)b(\xi) & (\xi > \xi_c). \end{cases} \quad (4.26)$$

Thus, we get the effective equation

$$\begin{cases} \dot{X} = \mathcal{L}X + K^* * X + L^* * Y, \\ \dot{Y} = \mathcal{L}Y + M^* * X + N^* * Y, \end{cases} \quad (4.27)$$

where $K^*(x) := \mathcal{F}^{-1}(\tilde{v}_1^*(\xi))(x)$, $L^*(x) := \mathcal{F}^{-1}(\tilde{p}^*(\xi))(x)$, $M^*(x) := \mathcal{F}^{-1}(\tilde{q}^*(\xi))(x)$, $N^*(x) := \mathcal{F}^{-1}(\tilde{v}_2^*(\xi))(x)$ and the differential operator $\mathcal{L} := \mathcal{F}^{-1}(\lambda_h(\xi))$.

Practical way II):

In (4.4), we use $B'_\varepsilon(\xi) := e^{-\varepsilon \xi^2} B_h(\xi)$ instead of $B_\varepsilon(\xi)$. Then all eigenvalues $\zeta'_j(\xi)$ of $B'_\varepsilon(\xi)$ satisfy $\zeta'_j(\xi) \rightarrow 0$ as $|\xi| \rightarrow \infty$. Hence by adjusting ε and δ appropriately such that $Re(\zeta'_j(\xi)) > -1/\delta$, we may take $\mu = \zeta'_j(\xi)$ as the solution of (4.7). Actually, $M_{max}(z) = z$ holds for $z \in \mathbf{C}$ with $Re(z) > -1/\delta$ and $|Im(z)| \leq C$ for $C > 0$ when $0 < \delta \ll 1$. Consequently, we can simply take $\mu'_{max}(\xi) := \max_j \{Re(\zeta'_j(\xi))\}$ instead of $\mu_{max}(\xi)$. In particular, $\mu'_{max}(\xi) = \max_j \{\zeta'_j(\xi)\}$ when $\zeta'_j(\xi) \in \mathbf{R}$. In Fig.10, the kernel $K'(x) = \mathcal{F}^{-1}(\mu'_{max}(\xi))(x)$ is drawn under the same parameters as Fig.8. It suggests that the essential structure of the original kernel $K(x)$ is retained by this rough approximation.

In the case of complex $\zeta'_j(\xi)$ as in Section 4.2, we define $b'(\xi)$, $\omega'_j(\xi)$ and $\tilde{\omega}'_j(\xi)$ for $\zeta'_j(\xi)$ in the same manners as $b(\xi)$, $\omega_j(\xi)$ and $\tilde{\omega}_j(\xi)$ for $\zeta_j(\xi)$. Then, we can take $\tilde{\mu}'_j(\xi) = \tilde{\omega}'_j(\xi)$ in (4.16), that is, $\tilde{\mu}'_1(\xi) = \omega'_1(\xi) + ib'(\xi)$ and $\tilde{\mu}'_2(\xi) = \omega'_2(\xi) - ib'(\xi)$. Now we can calculate $\tilde{p}'(\xi)$, $\tilde{v}'_j(\xi)$ and $\tilde{q}'(\xi)$ corresponding to $\tilde{p}(\xi)$, $\tilde{v}_j(\xi)$ and $\tilde{q}(\xi)$ respectively as follows:

Since $\tilde{\mu}'_j(\xi) = \zeta'_j(\xi)$ for $\xi < \xi_c$ and $\tilde{\mu}'_1(\xi) = \overline{\tilde{\mu}'_2(\xi)} = a'(\xi) + ib'(\xi)$ for $\xi > \xi_c$, we see $\tilde{a}'(\xi) = a'(\xi)$, $\tilde{b}'(\xi) = b'(\xi)$ and therefore we get

$$\tilde{p}'(\xi) := \begin{cases} \frac{\tilde{\mu}'_2(\xi) - \tilde{\mu}'_1(\xi)}{\zeta'_2(\xi) - \zeta'_1(\xi)} = 1 & (\xi < \xi_c), \\ \tilde{p}'_c := 1 & (\xi = \xi_c), \\ \frac{\tilde{b}'(\xi)}{b'(\xi)} = 1 & (\xi > \xi_c), \end{cases} \quad (4.28)$$

$$\tilde{v}'_j(\xi) := \begin{cases} \tilde{\mu}'_j(\xi) = \zeta'_j(\xi) & (\xi \leq \xi_c), \\ \tilde{a}'(\xi) = a'(\xi) & (\xi > \xi_c), \end{cases} \quad (4.29)$$

and

$$\tilde{q}'(\xi) := \begin{cases} 0 & (\xi \leq \xi_c), \\ -\tilde{b}'(\xi)b'(\xi) = -\{b'(\xi)\}^2 & (\xi > \xi_c). \end{cases} \quad (4.30)$$

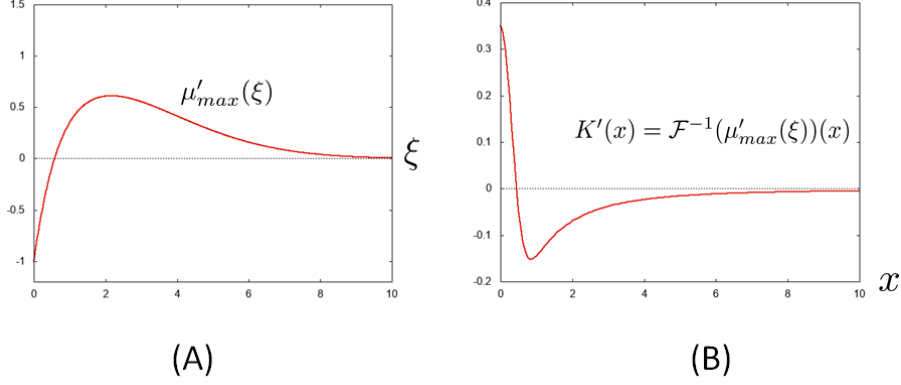


Figure 10: (A) Graph of $\mu'_{max}(\xi) = \max_j \{\zeta'_j(\xi)\}$ for the eigenvalues $\zeta'_j(\xi)$ of $B'_\varepsilon(\xi)$. (B) The derived kernel $K'(x) = (\mathcal{F}^{-1} \mu'_{max})(x)$, which shows the Mexican hat profile. Parameters are same as those of Fig.6, Fig.8 and Fig.9: $c_1 = c_2 = 1$, $c_3 = 4$, $c_4 = 3$, $d_1 = 0.05$, $d_2 = 3$ and $\varepsilon = 0.05$. Only the right half pictures are drawn both in (A) and (B).

Thus, the effective equation is obtained as

$$\begin{cases} \dot{X} &= \mathcal{L}X + K' * X + Y, \\ \dot{Y} &= \mathcal{L}Y + M' * X + N' * Y, \end{cases} \quad (4.31)$$

where $K'(x) := \mathcal{F}^{-1}(\tilde{v}'_1(\xi))(x)$, $M'(x) := \mathcal{F}^{-1}(\tilde{q}'(\xi))(x)$, $N'(x) := \mathcal{F}^{-1}(\tilde{v}'_2(\xi))(x)$ and the differential operator $\mathcal{L} := \mathcal{F}^{-1}(\lambda_h(\xi))$.

5. Applications

In previous sections, we only dealt with 1D problems just for simplicity while 2D problems should be considered as more realistic situations. Hence, some of the following applications, we consider 1D and 2D problems. In 2D case, ∂_x^2 is replaced with the Laplacian $\Delta = \partial_x^2 + \partial_y^2$ and the Heat kernel $H_\varepsilon(x)$ on 1D is done with $H_\varepsilon(\mathbf{x}) = \frac{1}{4\pi\varepsilon} e^{-\frac{r^2}{4\varepsilon}}$ for $\mathbf{x} = (x, y) \in \mathbf{R}^2$, $r = \sqrt{x^2 + y^2}$ and so on.

The numerical simulations on spatial patterns are done by using the equation

$$u_t = \mathcal{L}u + \chi(u) \cdot (K_j * u), \quad (5.1)$$

where $K_j = K_1(x)$ (1D kernel) or $K_2(x, y)$ (2D kernel) and \mathcal{L} , the derived kernels and differential operator in the manner of this paper, and $\chi(u)$ is a cut-off function satisfying $0 \leq \chi(u) \leq 1$ and $\chi(u) = 0$ for $|u| \geq u^*$ as in Figure 11.

5.1. Three node reaction-diffusion network

In this subsection, we consider the three node network as in Figure 12 dealt with in [14] as Type III network. The typical property of this example is that v and w diffuse with the same diffusion coefficients $d > 0$ and u does not move. In order to derive an effective kernel of this network,

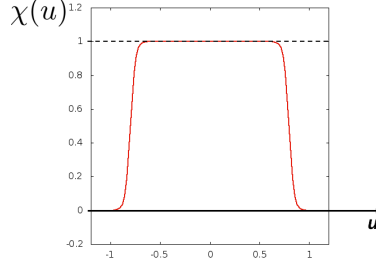


Figure 11: An example of the functional form of $\chi(u)$ in the case of $u^* = 1$.

we use the notations in Section 2. Let $U = {}^t(u, v, w)$. In this network, the diffusion matrix D is given by $D = \text{diag}\{0, d, d\}$. The matrix A describing the network is $A = \begin{pmatrix} 0 & k_2 & 0 \\ k_3 & -k_4 & -k_6 \\ k_7 & 0 & -k_9 \end{pmatrix}$. Then the corresponding equation to (4.2) leads $\widehat{U}_t = B(\xi^2)\widehat{U}$ in 1D and $\widehat{U}_t = B(R^2)\widehat{U}$ in 2D with $R = \sqrt{\xi^2 + \eta^2}$, where

$$\begin{aligned} B(s) &= -sD + A \\ &= -s\text{diag}\{0, d, d\} + A \\ &= \begin{pmatrix} 0 & k_2 & 0 \\ k_3 & -ds - k_4 & -k_6 \\ k_7 & 0 & -ds - k_9 \end{pmatrix} \end{aligned}$$

for $s = \xi^2$ or $s = R^2$ depending on the spatial dimension. Letting $\lambda_j(s)$ ($j = 1, 2, 3$) be eigenvalues of $B(s)$, we see $\lambda_{\max}(s) := \max_j \{\lambda_j(s)\} \rightarrow c$ as $s \rightarrow \infty$ for $c \in \mathbf{R}$. Hence by virtue of the way in Section 4.1, we take $\lambda_h(s) = 0$ and $B_h(s) = B(s)$. Since $B_h(s) = -sD + A$, we should deal with $B_\varepsilon(s) = -sD + e^{-\varepsilon s}A$ for $0 < \varepsilon \ll 1$ by the manner stated in Section 4.1. But here we use a simpler way stated in Practical way II) and put $B'_\varepsilon(s) = e^{-\varepsilon s}B_h(s)$. Then $\mu'_{\max}(s)$ is given by $\mu'_{\max}(s) = \max_j \{\zeta'_j(s) \in \sigma(B'_\varepsilon(s))\}$.

In Fig.13, the first, second and third maximal eigenvalues of $B'_\varepsilon(s)$ are drawn and also the 1D and 2D kernels $K'_1(x) = \mathcal{F}^{-1}(\mu'_{\max}(\xi^2))(x)$ and $K'_2(r) = \mathcal{F}^{-1}(\mu'_{\max}(R^2))(r)$, which shows that the effective kernel $K'_j(x)$ has a Mexican hat profile and we can understand the LALI effect essentially occurs even if the diffusion constants are same.

5.2. Two node reaction-diffusion network with long range interaction

We apply the method to a problem including long range interaction in the network, which was stated in [15], [22] for interactions between zebra-fish pigment cells. The schematic picture of the network is like Fig.14. The long range interaction means a cell interact directly to cells at a constant distant location by e.g. projections as in Figure 4 and we may represent the effect by the kernel $L_l(x) := \frac{1}{2}\{\delta(x+l) + \delta(x-l)\}$ for $x \in \mathbf{R}$ and $L_l(x, y) := \frac{1}{2\pi l}\delta(|\mathbf{x}| - l)$ for $\mathbf{x} = (x, y) \in \mathbf{R}^2$, where l is a positive constant. Let u and v be the differences from some rest states of densities of the two types of pigment cells, melanophores and xanthophores, respectively ([15]). Then the

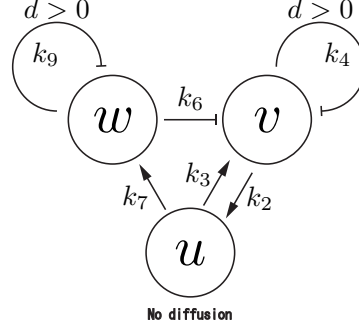


Figure 12: Three node network. The picture is cited from [14] with the same notations as in Appendix 3-figure 4 in [14].

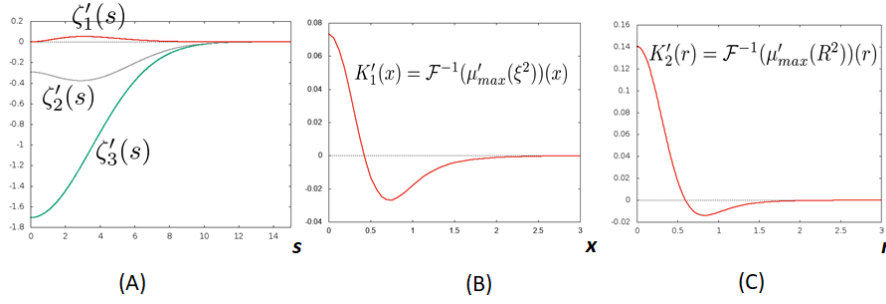


Figure 13: (A) Eigenvalues of $B'_\epsilon(s)$, (B) The kernel $K'_1(x) = \mathcal{F}^{-1}(\mu'_{max}(\xi^2))(x)$ on 1D, (C) The kernel $K'_2(r) = \mathcal{F}^{-1}(\mu'_{max}(R^2))(r)$ on 2D. Parameter values are $k_2 = 0.5$, $k_3 = k_4 = k_6 = k_7 = k_9 = 1$, $d = 0.02$ and $\epsilon = 0.05$. All values except ϵ are same as in Appendix 3-figure 4 in [14].

matrix A describing the network according to Fig.14 is

$$AU = \begin{pmatrix} -k_1 L_l * -k_5 & -k_3 + k_4 L_l * \\ -k_2 & -k_6 \end{pmatrix} U = \begin{pmatrix} -k_1 L_l * u - k_5 u - k_3 v + k_4 L_l * v \\ -k_2 u - k_6 v \end{pmatrix}$$

for $U = {}^t(u, v)$. In [15], it was simulated with the same small diffusion constants of u and v . Hence we also assume u and v spatially diffuse with the same diffusion constant d . Then the corresponding equation to (4.1) is

$$U_t = D\Delta U + AU,$$

where $D = \text{diag}\{d, d\}$. Taking the Fourier transformation of the above equation, we have

$$\hat{U}_t = B_1(\xi)\hat{U} \quad (1D \text{ case}), \quad \hat{U}_t = B_2(R)\hat{U} \quad (2D \text{ case}),$$

where $R = \sqrt{\xi^2 + \eta^2}$ and

$$B_j(s) = \begin{pmatrix} -ds^2 - k_1 \hat{L}_l(s) - k_5 & -k_3 + k_4 \hat{L}_l(s) \\ -k_2 & -ds^2 - k_6 \end{pmatrix}$$

for $s = \xi$ in 1D or $s = R$ in 2D. Here, \hat{L}_l is computed for 1D,

$$\hat{L}_l(\xi) = \frac{1}{2}(e^{i\xi l} + e^{-i\xi l})\hat{\delta}(\xi) = \cos \xi l =: P_1(\xi)$$

and for 2D,

$$\frac{1}{2\pi l} \widehat{L}_l(R) = \int_0^\infty \int_0^{\pi/2} r \delta(r-l) \cos(rR \sin \theta) d\theta dr = \frac{1}{2\pi} \int_0^{\pi/2} \cos(lR \sin \theta) d\theta =: P_2(R)$$

by using (5.1). Thus we find

$$B_j(s) = \begin{pmatrix} -ds^2 - k_1 P_j(s) - k_5 & -k_3 + k_4 P_j(s) \\ -k_2 & -ds^2 - k_6 \end{pmatrix}$$

satisfying $B_j(-s) = B_j(s)$.

Let $\lambda_{1,j}(s)$ and $\lambda_{2,j}(s)$ be eigenvalues of $B_j(s)$. Since eigenvalues have the asymptotic profile in the highest order of s as $\lambda_{i,j}(s) \rightarrow -ds^2 + O(1)$ as $s \rightarrow \infty$, we take $\lambda_h(s) = -ds^2$ and $B_{j,h}(s) = \{B_j(s) + ds^2 I\}$ according to Section 4.1. Since $B_{j,h}(s) = O(1)$, we put $B_{j,\varepsilon}(s) = e^{-\varepsilon s^2} B_{j,h}(s)$. Then $\mu_{\max}(s)$ may be calculated by using the approximation stated in Practical way II) as $\mu_{\max}(s) = \max_j \{\zeta_{i,j}(s) \in \sigma(B_{i,\varepsilon}(s))\}$ and we get the effective equation by

$$(1D) : w_t = dw_{xx} + K_1 * w, \quad (2D) : w_t = d\Delta w + K_2 * w.$$

In Fig.15, $\mu_{\max}(s)$ of $B_1(s)$ and $B_2(s)$ are respectively drawn together with the reduced kernels in 1D and 2D for the case corresponding to the simulation in [15]. Fig.16 and Fig.17 are numerical simulations for 2D patterns by using the reduced equation $w_t = d\Delta w + \chi(w) \cdot (K_2 * w)$ with the kernel $K_2(r)$ in Fig.15, which shows that the similar patterns to [15] appear. Here, we should note that the system of u and v without long range interactions (corresponding to the case of $k_1 = k_4 = 0$ in Figure 14) is unstable in the kinetics, that is, the matrix $\begin{pmatrix} -k_5 & -k_3 \\ -k_2 & -k_6 \end{pmatrix}$ has eigenvalues with positive real parts under the parameter values in Figure 15. In [15], it was demonstrated that the Turing pattern appears by introducing the third component w , which plays the role of long range interactions. In this subsection, the long range interactions are directly introduced by L_l and the Turing pattern is naturally observed in 2D as in (C) of Figure 15, that is, $\lambda_1(0) < 0$ in (C). Thus, the method in this paper does not require any artificial treatment and make the direct understanding of the mechanism possible through the reduced kernels.

Remark 5.1. In Fig.15 (A), we observe $\lambda_1(0) > 0$, which means that the Turing pattern does not appear in 1D case for any $l > 0$. Actually, the functional form of $P_1(\xi) \sim 2 \cos \xi l$ leads $P_1(0) = 2$ independent of l and the matrix $B_1(0)$ has a positive eigenvalue under the parameter values in Fig.15 while in 2D, $P_2(0) = 2\pi l$ holds and the maximal eigenvalue $\lambda_1(0)$ of $B_2(0)$ can be negative depending on l .

In the last of this subsection, we show numerical simulations comparing two cases of $k_1 \neq 0$ and $k_1 = 0$ because the self-inhibition of u component is not assumed in [22]. Fig.18 shows the comparison of eigenvalues and the reduced kernels between the cases $k_1 \neq 0$ and $k_1 = 0$. Fig.19 and Fig.20 show the numerical simulations in 2D patterns under the parameters of Fig.18. They strongly suggest that two situations with nonzero and zero k_1 values exhibit almost same properties with respect to reduced kernels and 2D patterns.

5.3. Network for Proneural waves

It was reported in [20] that regulated waves of differentiation called the ‘‘proneural wave’’ is observed in visual systems on the surface of the brain of the fruit fly. The phenomena was modeled in a mathematical PDE model as the Delta-Notch system including variables E , N , D and

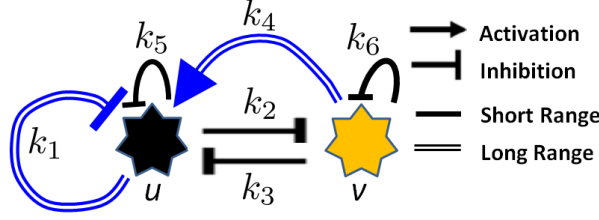


Figure 14: Deduced interaction network between pigment cells of Zebra-fish, which is referred from [15, 22]. The coefficient k_1 is possibly equal to zero ([22]).

A_s corresponding to the EGF ligand concentration and EGF signaling (E), Notch signal activity (N), Delta expression (D) and the level of the differentiation of AS-C in cells (A_s), respectively. The network of the molecular interactions is as in Fig.21 (B). The typical properties of the network is that E diffuses and other materials do not and that D inhibits N in the same cell while it activates N in contiguous cells (Fig.21 (C)). Then by denoting the distance between a cell and the contiguous cells by $l > 0$, the matrix A describing the network drawn in Fig.21 is given by

$$AU = \begin{pmatrix} -k_e & 0 & 0 & a_e \\ 0 & -k_n & d_l L_l * -d_c & 0 \\ 0 & 0 & -k_d & a_d \\ e_a & -e_a & 0 & 0 \end{pmatrix} U = \begin{pmatrix} -k_e E + a_e A_s \\ -k_n N + d_l L_l * D - d_c D \\ -k_d D + a_d A_s \\ e_a (E - N) \end{pmatrix}$$

for $U = {}^t(E, N, D, A_s)$. Here we used the same functions and notations as those in the previous subsections such as $P_j(s)$. The equation is

$$U_t = D\Delta U + AU,$$

where $D = \text{diag}\{d_e, 0, 0, 0\}$. The Fourier transformation leads $\hat{U}_t = B_1(\xi)\hat{U}$ (1D case) and $\hat{U}_t = B_2(R)\hat{U}$ (2D case), where $R = \sqrt{\xi^2 + \eta^2}$, $B_j(s) = -s^2 D + \hat{A}_j(s)$ and

$$\hat{A}_j(s) = \begin{pmatrix} -k_e & 0 & 0 & a_e \\ 0 & -k_n & d_l P_j(s) - d_c & 0 \\ 0 & 0 & -k_d & a_d \\ e_a & -e_a & 0 & 0 \end{pmatrix}.$$

Since the maximal eigenvalue of $B_j(s)$ is $O(1)$, we take $\lambda_h(s) = 0$, $B_{j,h}(s) = B_j(s) = -s^2 D + \hat{A}_j(s)$ with $\hat{A}_j(s) = O(1)$ and therefore we should put $B_{j,\varepsilon}(s) = -s^2 D + e^{-\varepsilon s^2} \hat{A}_j(s)$ according to the manner in Section 4. But, here we use the simplest case of $B'_{j,\varepsilon}(s) = e^{-\varepsilon s^2} B_{j,h}(s)$ according to Practical way II) and only consider 2 dimensional problems (the case of $s = R = \sqrt{\xi^2 + \eta^2}$). The effective equations are as follows:

When all eigenvalues $\zeta'_j(R)$ of $B'_{j,\varepsilon}(R)$ are real, the effective equation is $w_t = K'_2 * w$, where $K'_2(r) = \mathcal{F}^{-1}(\mu'_{\max}(R))(r)$ and $\mu'_{\max}(R) = \max_j \{\zeta'_j(R)\}$ for $r = \sqrt{x^2 + y^2}$. In numerical simulations, the equation

$$w_t = \chi(w) \max\{ \cdot (K'_2 * w), 0 \} \quad (5.2)$$

is treated because of the irreversibility of the differentiation of cells, which will require the monotonicity in time and the modification in (5.2) seems natural. In Fig.22, $\mu'_{\max}(R)$ and the reduced

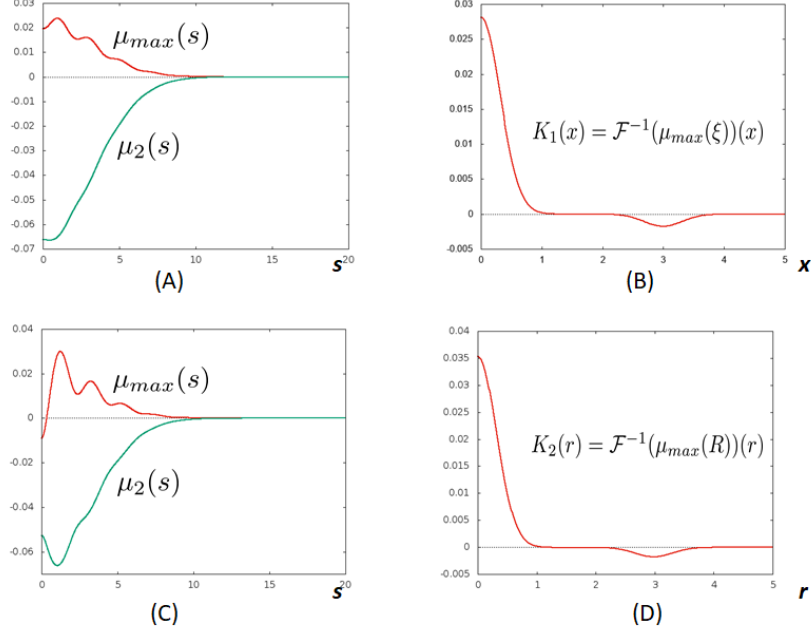


Figure 15: (A) $\mu_{max}(s)$ of $B_1(s)$, (B) The kernel $K_1(x) = \mathcal{F}^{-1}(\mu_{max}(\xi))(x)$ by $B_1(s)$, (C) $\mu_{max}(s)$ of $B_2(s)$, (D) The kernel $K_2(r) = \mathcal{F}^{-1}(\mu_{max}(R))(r)$ by $B_2(s)$. Parameters are $d = 0.02$, $k_1 = 0.055 * 0.016$, $k_2 = 0.05$, $k_3 = 0.04$, $k_4 = 0.055 * 0.03$, $k_5 = 0.02$, $k_6 = 0.025$. which are adjusted to parameter values for a wild type of Fig 4 in [15]. l and ε are given by $l = 3$ and $\varepsilon = 0.05$.

kernel are drawn in the case that eigenvalues of $B'_{j,\varepsilon}(s)$ are all real. Fig.23 draws the numerical simulation of (5.2) by using the kernel $K'_2(r)$ in Fig.22. It shows a stable traveling planar pattern appears corresponding to the proneural wave.

When the eigenvalue with maximal real part can be complex, we get (4.31) with $\mathcal{L} = \mathcal{F}^{-1}(\lambda_h(R)) = 0$. that is

$$\begin{cases} \dot{X} &= K'_2 * X + Y, \\ \dot{Y} &= M'_2 * X + N'_2 * Y, \end{cases}$$

where $K'_2(r) = \mathcal{F}^{-1}(\tilde{v}'_1(R))(r)$, $M'_2(r) = \mathcal{F}^{-1}(\tilde{q}'(R))(r)$ and $N'_2(r) = \mathcal{F}^{-1}(\tilde{v}'_2(R))(r)$. Numerical simulations are done by the following equation:

$$\begin{cases} \dot{X} &= \chi(X) \max\{(K'_2 * X + Y), 0\}, \\ \dot{Y} &= \chi(Y)(M'_2 * X + N'_2 * Y) \end{cases} \quad (5.3)$$

because of the irreversibility of the differentiation of cells as stated for (5.2). In Fig.24, the reduced kernels $K'_2(r)$, $M'_2(r)$ and $N'_2(r)$ are shown in the case when $B'_{2\varepsilon}(R)$ can have complex eigenvalues. The parameter values are same as those of Fig.22 except the coefficient a_e . In practice, $a_e = 1$ in Fig.22 and $a_e = 0.1$ in Fig.24. As in Fig.21 and also in the matrix A , a_e denotes the activation rate of A_s (AS-C) for E (EGF). Lower a_e is expected to enhance the lateral inhibition by Delta/Notch signaling shown in Fig.21 (C) and as the consequence, pepper and salt patterns are caused as indicated in [20]. Fig.25 demonstrates the occurrence of salt and pepper patterns.

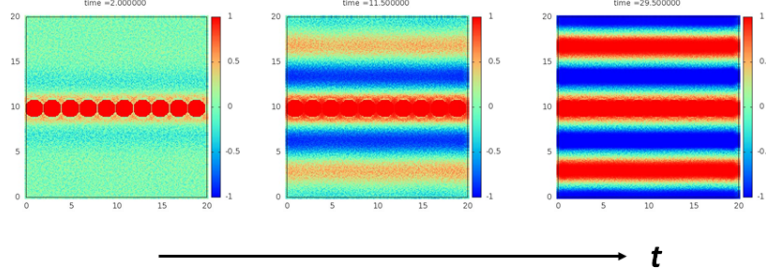


Figure 16: Time evolution of spatial patterns in 2D by the kernel $K_2(r)$ in Fig.15 (D) using (5.1) with $u^* = 1$. The initial condition is set similarly to that of the numerical simulations reported in [15].

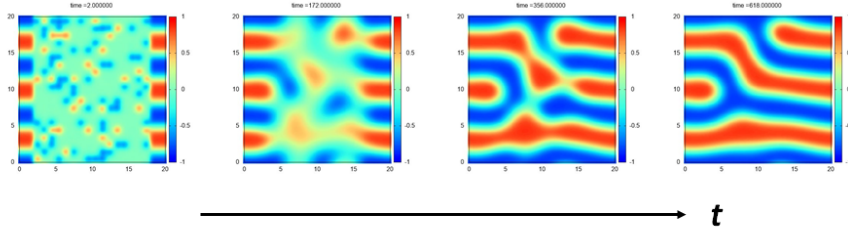


Figure 17: Time evolution of spatial patterns in 2D with initial data added a random ablated region by the kernel $K_2(r)$ in Fig.15 (D) using (5.1) with $u^* = 1$.

Remark 5.2. In this section, we adopted the heat kernel $H_\varepsilon(x)$ as the approximation of the Dirac δ -function. If zero state is unstable as the grand state in a system, the approximation by the heat kernel may cause some trouble because the heat kernel H_ε activates the instability everywhere by the property that $(H_\varepsilon * u)(x) > 0$ everywhere for a function $u(x) \geq 0$. In that case, the approximation by the mollifier J_ε stated in Proposition 2.1 seems better because the mollifier can approximate supports, i.e., the support of $J_\varepsilon * u$ is close to the support of u . Then, we can replace $B_{j,\varepsilon}(s)$ either by $B_{j,\varepsilon}^*(s) = -s^2 D + \widehat{J}_\varepsilon(s) \cdot \widehat{A}_j(s)$ or roughly $B'_{j,\varepsilon}(s) = \widehat{J}_\varepsilon(s) \cdot B_j(s) = \widehat{J}_\varepsilon(s) \cdot \{-s^2 D + \widehat{A}_j(s)\}$.

6. Discussion

The efficiency of KT models for the investigation of spatial patterns in biology was clearly mentioned in [8]. In this paper, we proposed a method to get the effective kernels from given network systems. Patterns generated from network systems are directly determined by the reduced kernels. It means even when given two network systems seem quite different each other, the two different network systems can be identified from the view point of patterns through the reduced effective kernels. The application stated in 5.1 is a typical example of that point. In practice, the effective kernel of the network of Fig.12 has a Mexican hat profile as in Fig.13 with LALI effect similar to the kernel mentioned in Section 3 and we can regard the generated pattern as a usual Turing pattern. Thus we can classify network systems through effective kernels from the pattern formation point of view.

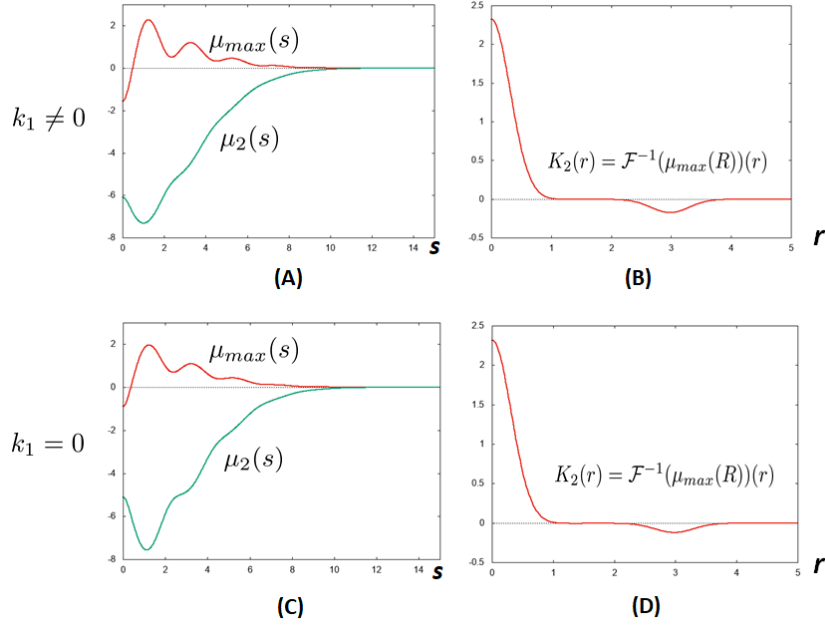


Figure 18: Comparison between the cases of $k_1 = 5.5 * 0.016 \neq 0$ and $k_1 = 0$. Other parameters are fixed by $l = 3.0$, $d = 0.2$, $k_2 = 5.0$, $k_3 = 4.0$, $k_4 = 5.5 * 0.03$, $k_5 = 3.0$, $k_6 = 3.0$. For $k_1 = 5.5 * 0.05$, (A) eigenvalues of $B_2(s)$, (B) the kernel $K_2(r) = \mathcal{F}^{-1}(\mu_{max}(R))(r)$. For $k_1 = 0$, (C) eigenvalues of $B_2(s)$, (D) the kernel $K_2(r) = \mathcal{F}^{-1}(\mu_{max}(R))(r)$.

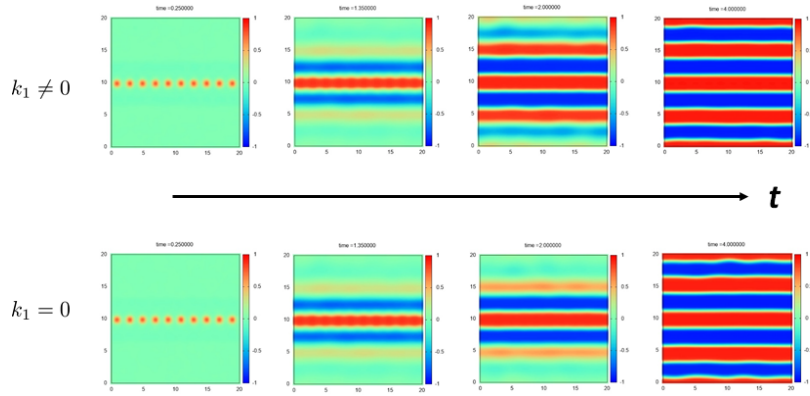


Figure 19: Comparison between the cases of $k_1 = 5.5 * 0.016 \neq 0$ and $k_1 = 0$. Other parameters are fixed under the parameters of Fig.18. The upper picture is a time evolutionary 2D pattern with the kernel $K_2(r)$ of Fig.18 (B) and the lower picture is the one with the kernel $K_2(r)$ of Fig.18 (D). The initial data is the same one as Fig.16.

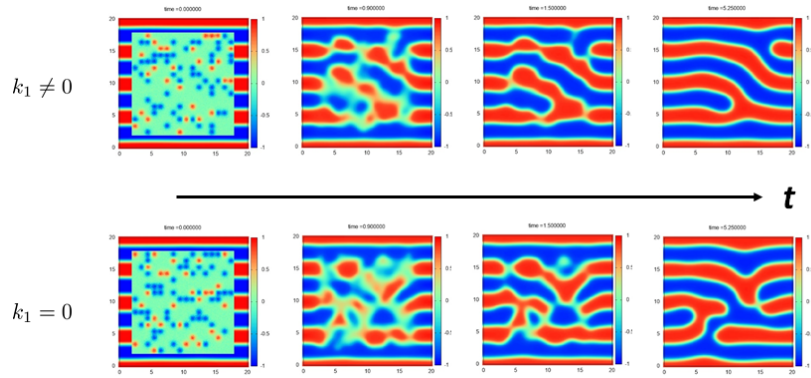


Figure 20: Comparison between the cases of $k_1 = 5.5 * 0.016 \neq 0$ and $k_1 = 0$. Other parameters are fixed under the parameters of Fig.18. The upper picture is a time evolutionary 2D pattern with the kernel $K_2(r)$ of Fig.18 (B) and the lower picture is the one with the kernel $K_2(r)$ of Fig.18 (D). The initial data is the same one as Fig.17 added a random ablated region.

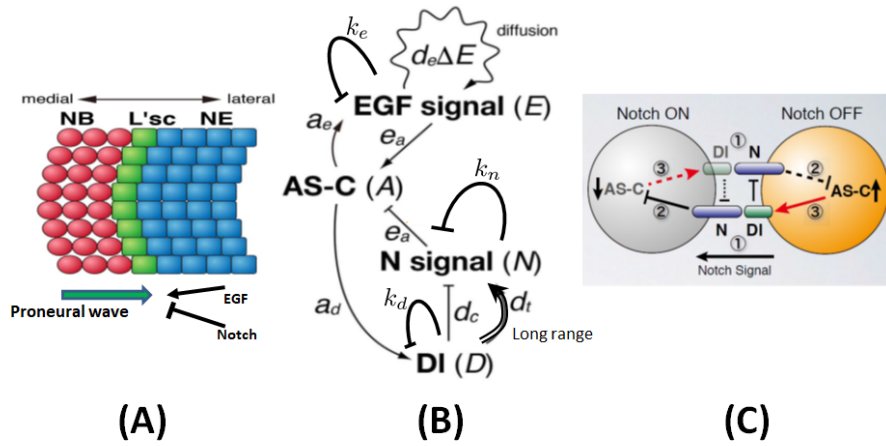


Figure 21: The proneural wave progresses unidirectionally during optic lobe development in *Drosophila*. (A) A schematic of the progression of the proneural wave. The proneural wave sweeps from medial to lateral. L'sc is transiently expressed in the differentiating neuroepithelial cells (NEs) and defines the timing of the differentiation of the NE to the neuroblast (NB). EGF positively regulates the progression of the wave, while Notch negatively regulates wave progression through increasing the expression of Notch target genes. (B) Schema showing the gene regulatory network including AS-C, EGF, Notch and Delta. (C) Lateral inhibition mechanism of Delta/Notch signaling.

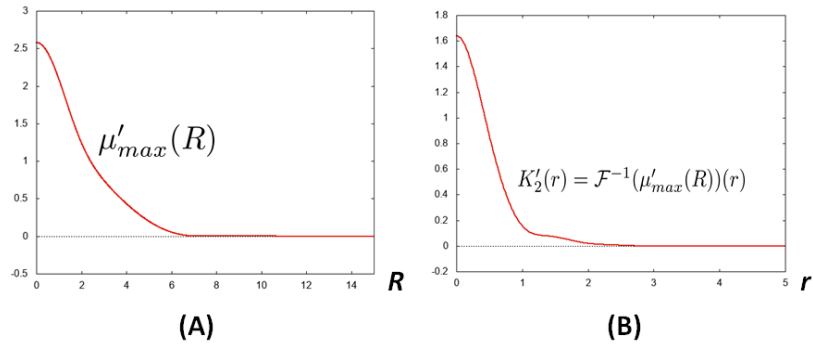


Figure 22: (A) $\mu'_{max}(R)$ obtained from $B'_{2,\varepsilon}(s)$. (B) The reduced kernel from $\mu'_{max}(R)$. The parameter values are $d_e = 1.0$, $k_e = 1.0$, $a_e = 1.0$, $k_n = 2.0$, $d_t = 0.5/(2\pi l)$, $d_c = 0.1$, $k_d = 1.5$, $a_d = 1.0$ and $e_d = 10.0$. We also take $l = 1$ and $\varepsilon = 0.05$.

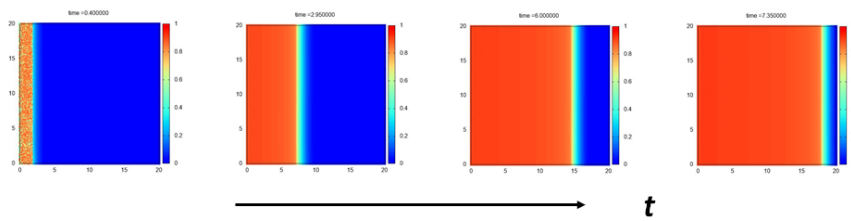


Figure 23: Time evolution of spatial pattern in 2D simulated by (5.2) with the kernel $K'_2(r)$ of Fig.22, which shows a regulated propagation of proneural wave. Red color means the higher value of w . Parameter values are same as those in Fig.22.

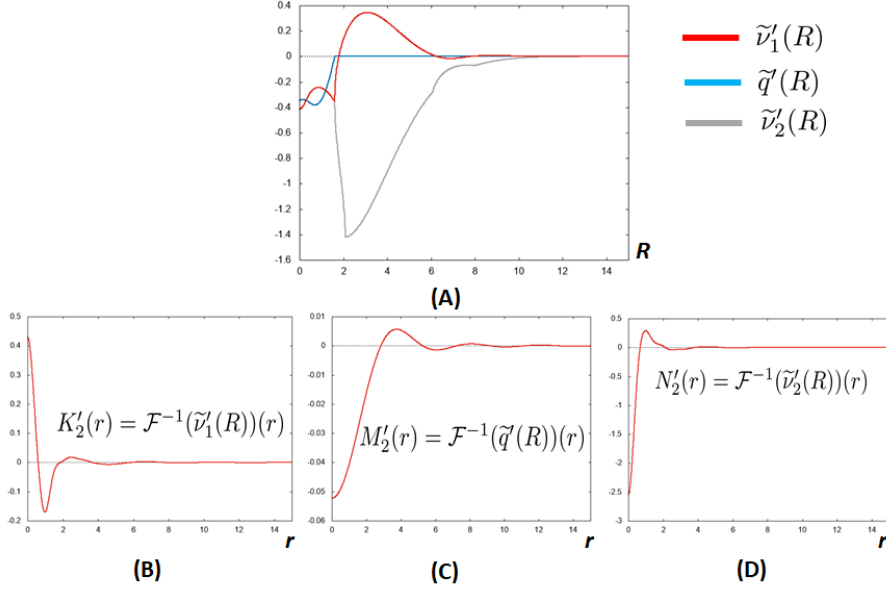


Figure 24: (A) $\tilde{v}'_1(R)$, $\tilde{v}'_2(R)$ and $\tilde{q}'(R)$ obtained from $B'_{2,\varepsilon}(R)$. (B), (C), (D) are the kernels obtained from them. The parameter values are $d_e = 1.0$, $k_e = 1.0$, $a_e = 0.1$, $k_n = 2.0$, $d_r = 0.5/(2\pi l)$, $d_c = 0.1$, $k_d = 1.5$, $a_d = 1.0$ and $e_a = 10.0$. We also take $l = 1.0$ and $\varepsilon = 0.05$. Only a_e is changed smaller than the one in Fig.22 and Fig.23.

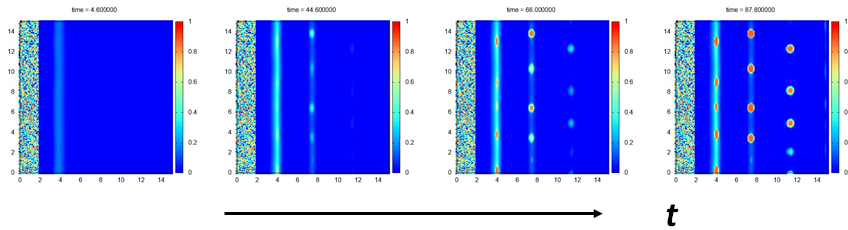


Figure 25: Time evolution of spatial pattern in 2D simulated by (5.3) with kernels K'_2 , M'_2 and N'_2 computed in (B), (C) and (D) of Fig.24, which shows salt and pepper patterns. Only X component is drawn. Parameter values are same as those of Fig.24.

Other point of this paper is to propose a new method for modeling of phenomena. Two applications given in 5.2 and 5.3 are demonstrations of it. In fact, we can observe the reproduction of the same patterns in Fig.16 and Fig.17 as the patterns simulated by using a corresponding mathematical model in [15] and also the same traveling planar and/or salt-pepper patterns in Fig.22 and Fig.25 as the patterns in [20]. It means that we can propose a new method to make mathematical models describing phenomena in the types of (5.1) and (5.3) by using effective kernels.

Of course, the model equations in types of (5.1) and (5.3) have advantages and disadvantages compared with standard model equations. One advantage is the systematic and routine derivation of equations for given network systems while the construction of model equations in standard manners requires a deep understanding on the underlying mechanism of patterns and careful adjustments of nonlinearities. The possibility of classification of patterns by kernels is another advantage. The disadvantage is that the meaning of variables in the equations are not clear by the big reduction from original systems. Moreover, the equations of (5.1) and (5.3) are reduced from the linearized systems of given network systems and therefore they can not include nonlinear effects, which is also disadvantage. Thus, the model equations in types of (5.1) and (5.3) and model equations derived in standard manners should be complementary to each other.

Finally, we mention about how to detect the kernel shape from the observation in real experiments. We apply the Practical way II directly to (4.2) as the simplest way, that is, define $B_\varepsilon(\xi) = e^{-\varepsilon\xi^2}B(\xi)$ and $\mu_{max}(\xi) = \max_j\{\zeta_j(\xi) \in \sigma(B_\varepsilon(\xi))\}$ by assuming $\zeta_j(\xi) \in \mathbf{R}$. Then the effective equation is $u_t = K * u$, where $K(x) = \mathcal{F}^{-1}(\mu_{max}(\xi))(x)$. The kernel $K(x)$ is detected by experiments as follows: Since $\hat{u}(t + \delta, \xi) = e^{\delta\hat{K}(\xi)}\hat{u}(t, \xi) = (1 + \delta\hat{K}(\xi) + O(\delta^2))\hat{u}(t, \xi)$ holds for any $t > 0$ and $0 < \delta \ll 1$, we see $\hat{K}(\xi) = \frac{1}{\delta} \left(\frac{\hat{u}(t + \delta, \xi)}{\hat{u}(t, \xi)} - 1 \right) + O(\delta)$. This implies practically that the ratio of the Fourier transformations of two profiles, a profile at time t and the one after short time directly gives the kernel shape by focusing on an arbitrarily fixed element of the network.

Acknowledgment

The authors thank Akiko Nakamasu (Kumamoto University, Japan) for her helpful discussion.

References

- [1] S. Amari, Dynamics of Pattern Formation in Lateral-Inhibition Type Neural Fields, *Biol. Cybernetics* 27 (1977), 77-87.
- [2] P. W. Bates and F. Chen, Spectral analysis of traveling waves for nonlocal evolution equations, *SIAM J. Math. Anal.* 38, No. 1 (2006), 116-126.
- [3] P.W. Bates, X. Chen, A.J. J. Chmaj, Heteroclinic solutions of a van der Waals model with indefinite nonlocal interactions, *Calc. Var.* (2005) 24(3), 261-281, DOI 10.1007/s00526-005-0308-y
- [4] R.M. Corless, G.H. Gonnet, D.E.G. Hare, D.J. Jeffrey, D.E. Knuth, On the Lambert W function, *Advances in Computational Mathematics* 5 (1996), 329-359. doi:10.1007/BF02124750.
- [5] J. A. Carrillo, H. Murakawa, M. Sato, H. Togashi, O. Trush, A population dynamics model of cell-cell adhesion incorporating population pressure and density saturation, *J. Theor. Biology* 474 (2019), 14-24.
- [6] S.-I. Ei, M. Sato, Y. Tanaka, T. Yasugi, Continuous method for spatial discrete models with nonlocal interactions remaining cell or lattice size, submitted.
- [7] A. Gierer and H. Meinhardt, A theory of biological pattern formation, *Kybernetik* 12 (1972), 30-39.
- [8] S. Kondo, An updated kernel-based Turing model for studying the mechanisms of biological pattern formation, *Journal of Theoretical Biology* 414(2017), 120-127.

- [9] S. Kondo, R. Asai, A reaction-diffusion wave on the skin of the marine angelfish *Pomacanthus*, *Nature* 376(1995), 765-768.
- [10] S.W. Kuffler, Discharge patterns and functional organization of mammalian retina, *J. Neurophysiol.* 16 (1953), 37-68.
- [11] H. Meinhardt, 1982, *Models of Biological Pattern Formation*, Academic Press, London.
- [12] T. Miura, 2007. Modulation of activator diffusion by extracellular matrix in Turing system, *RIMS Kyokaku Bessatsu B3*, 12.
- [13] J. Murray, 2001. *Mathematical Biology*, Springer, USA.
- [14] L. Marcon, X. Diego, J. Sharpe, P. Muller, High-throughput mathematical analysis identifies Turing networks for patterning with equally diffusing signals, *eLife* 5(2016), DOI: 10.7554/eLife.14022.
- [15] A. Nakamasu, G. Takahashi, A. Kanbe and S. Kondo, Interactions between zebrafish pigment cells responsible for the generation of Turing patterns, *PNAS* 106 no. 21(2009), 8429-8434.
- [16] G.F. Oster, Lateral inhibition models of developmental processes. *Math. Biosci.* 90, 256-286(1988), [http://dx.doi.org/10.1016/0025-5564\(88\)90070-3](http://dx.doi.org/10.1016/0025-5564(88)90070-3).
- [17] Q. Ouyang and H. Swinney, Transition from a uniform state to hexagonal and striped Turing patterns, *Nature* 352(1991), 3.
- [18] K. J. Painter, J. M. Bloomfield, J. A. Sherratt, A. Gerisch, A nonlocal model for contact attraction and repulsion in heterogeneous cell populations, *Bulletin of Mathematical Biology.* 77, 6, 1132-1165
- [19] , T. Sushida, S. Kondo, K. Sugihara, and M. Mimura, A differential equation model of retinal processing for understanding lightness optical illusions, *Japan Journal of Industrial and Applied Mathematics*, 35(1) (2018), pp. 117-156.
- [20] M. Sato, T. Yasugi, Y. Minami, T. Miura, and M. Nagayama, Notch-mediated lateral inhibition regulates proneural wave propagation when combined with EGF-mediated reaction diffusion, *Proceedings of the National Academy of Sciences* 113, 35, E5153-E5162 (2016), 10.1073/pnas.1602739113.
- [21] A. M., Turing, The chemical basis of morphogenesis, *Philos. Trans. R. Soc. Lond. Ser. B* 237 (1952), 37 - 72.
- [22] M. Watanabe and S. Kondo, Is pigment patterning in fish skin determined by the Turing mechanism , *Trends in Genetics* Vol. 31 No. 2 (2015), 88-96. dx.doi.org/10.1016/j.tig.2014.11.005
- [23] M. Yamaguchi, E. Yoshimoto, S. Kondo, Pattern regulation in the stripe of zebrafish suggests an underlying dynamic and autonomous mechanism. *Proc. Natl. Acad. Sci. USA* 104(2007), 4790-4793, <http://dx.doi.org/10.1073/pnas.0607790104>.